

# PROVABLE GUARANTEES AGAINST DATA POISONING USING SELF-EXPANSION AND COMPATIBILITY

**Charles Jin**

CSAIL  
MIT  
Cambridge, MA 02139  
ccj@csail.mit.edu

**Melinda Sun**

MIT  
Cambridge, MA 02139  
mmsun@mit.edu

**Martin Rinard**

CSAIL  
MIT  
Cambridge, MA 02139  
rinard@csail.mit.edu

## ABSTRACT

As deep learning datasets grow larger and less curated, backdoor data poisoning attacks, which inject malicious poisoned data into the training dataset, have drawn increasing attention in both academia and industry.

We identify an *incompatibility property* of the interaction of clean and poisoned data with the training algorithm, specifically that including poisoned data in the training dataset does not improve model accuracy on clean data and vice-versa. Leveraging this property, we develop an algorithm that iteratively refines subsets of the poisoned dataset to obtain subsets that concentrate around either clean or poisoned data. The result is a partition of the original dataset into disjoint subsets, for each of which we train a corresponding model. A voting algorithm over these models identifies the clean data within the larger poisoned dataset.

We empirically evaluate our approach and technique for image classification tasks over the GTSRB and CIFAR-10 datasets. The experimental results show that prior dirty-label and clean-label backdoor attacks in the literature produce poisoned datasets that exhibit behavior consistent with the incompatibility property. The results also show that our defense reduces the attack success rate below 1% on 134 out of 165 scenarios in this setting, with only a 2% drop in clean accuracy on CIFAR-10 (and negligible impact on GTSRB).

## 1 OVERVIEW

Recent years have seen a rapid adoption of machine learning in a range of applications, from digital personal assistants to autonomous vehicles. A crucial driver has been the adoption of increasingly large, minimally curated training datasets gathered from a variety of sources. Such datasets open up the possibility of data poisoning attacks in which the attacker inserts malicious data during training to influence the quality of the learned model.

In this work, we focus on *backdoor data poisoning attacks* (Chen et al., 2017; Adi et al., 2018) against deep neural networks (DNNs). Specifically, by injecting a small amount of poisoned data into the training dataset, the attacker installs a backdoor in the network that can be used to control the network’s behavior at test time. For example, Gu et al. (2019) install a backdoor in a traffic sign classifier, which causes the network to misclassify stop signs as speed limit signs when a (physical) sticker is applied. Other triggers include a single pixel (Tran et al., 2018), small overlays such as a copyright symbol (Gao et al., 2019), or perturbations using adversarial training (Turner et al., 2018).

We present a new technique for identifying poisoned data within a dataset potentially containing both clean and poisoned data. Our technique leverages a property of the interaction of clean and poisoned data with the training algorithm—specifically, a model trained on clean data generalizes well to new clean data but poorly to poisoned data (and vice-versa). Building on this insight, we develop a technique that iteratively refines the dataset to separate clean and poisoned data into disjoint subsets.

The algorithm operates as follows. Given a dataset, the algorithm iteratively samples a subset of the dataset, trains a model on the subset, then selects the elements within the larger dataset that the model scores most highly. The selected elements comprise a smaller dataset for the next refinement step.

By decreasing the size of the selected subsets in each iteration, this process produces a final subset that (ideally) contains either clean data or poisoned data. The identified subset is then removed from the starting dataset, and the process is repeated to obtain a collection of refined subsets and corresponding trained models. Finally, a majority vote using models trained on the resulting refined clean and poisoned subsets distinguishes the clean and poisoned data in the initial training set.

We identify our main contributions as follows:

**Incompatibility of Clean and Poisoned Data.** Section 3 formally defines an *incompatibility property* that characterizes how clean and poisoned data interact with the training algorithm, specifically that training on clean data does not improve performance on poisoned data and vice-versa. Leveraging this property, we show that for poisoned datasets that satisfy the incompatibility property, the subset of the dataset that is “most compatible with itself” consists of either entirely clean or entirely poisoned data. We show that iteratively identifying such subsets based on this property provably separates the dataset into clean and poisoned components.

**Defense Mechanism.** While the iterative technique presented in Section 3 comes with a guarantee that it will always place clean and poisoned data into separate subsets (if the clean and poisoned data satisfy the incompatibility property), it is based on optimizing an objective that is intractable in practice. Section 4 therefore presents a technique that uses a heuristic to approximate the optimization objective from Section 3, thus obtaining a tractable defense mechanism.

**Experimental Evaluation.** Section 5 presents an empirical evaluation of the incompatibility property presented in Section 3 and the techniques developed in Section 4. The evaluation focuses on three different backdoor data poisoning attacks (two dirty label attacks using pixel-based patches and image-based patches, respectively, and a clean-label attack using adversarial perturbations) from the data poisoning literature (Gu et al., 2019; Gao et al., 2019; Turner et al., 2018). The results 1) indicate that the considered attacks produce poisoned datasets that satisfy the incompatibility property, 2) highlight the ability of our defense mechanism to effectively separate clean and poisoned data, and 3) demonstrate the ability of our technique to effectively identify poisoned data within a larger dataset containing both clean and poisoned data. For attacks against the GTSRB and CIFAR-10 datasets, our defense mechanism reduces the attack success rate to below 1% on 134 out of the 165 scenarios, with less than 2% drop in clean accuracy. In a comparison with three previous defenses against a standard dirty-label backdoor attack on the CIFAR-10 dataset, our defense successfully defends against 22 of the 24 scenarios, versus only 5 of the 24 scenarios for the next best defense.

## 2 PROBLEM SETTING

We formulate the backdoor data poisoning threat model in a binary classification setting. We first establish some basic notation. Let  $X$  be the input space,  $Y = \{-1, +1\}$  be the label space, and  $L(\cdot, \cdot)$  be the 0-1 loss function over  $Y \times Y$ , i.e.,  $L(y_1, y_2) = (1 - y_1 * y_2)/2$ . Given a target distribution  $\mathcal{D}$  supported on  $X \times Y$  and a parametric family of functions  $f_\theta$ , the objective is to find  $\theta$  minimizing the population risk  $R(\theta) := \int_{X \times Y} L(f_\theta(x), y) dP_{\mathcal{D}}(x, y)$ . Given  $n$  data points  $D = \{(x_1, y_1), \dots, (x_n, y_n)\}$ , the empirical risk is defined as  $R_{emp}(\theta; D) := n^{-1} \sum_{i=1}^n L(f_\theta(x_i), y_i)$ . We also fix a learning algorithm  $\mathcal{A}(\cdot)$  which takes as input a training set and returns parameters  $\theta$ . For example, if  $f_\theta$  is a family of DNNs, then  $\mathcal{A}$  might train a DNN via stochastic gradient descent.

### 2.1 THREAT MODEL

The attacker’s goal is to install a backdoor in the trained network that 1) changes the poisoned network’s predictions on poisoned data while 2) preserving the accuracy of the poisoned network on clean data. For the backdoor to be meaningful, the behavior of a poisoned model on poisoned data should also be inconsistent with a model trained on clean data.

We work with the standard model of statistical learning in which a set of  $n$  clean training samples  $D$  is drawn iid from  $\mathcal{D}$ . The attacker selects at most  $n/2 - 1$  samples  $A \subseteq D$  (leaving behind at least  $n/2$  clean samples  $C = D \setminus A$ ) and fixes a pair of perturbation functions  $\tau_{train} : X \times Y \mapsto X \times Y$  (the attacker uses  $\tau_{train}$  to construct the poisoned dataset for training, changing the image and potentially the label of each poisoned element) and  $\tau_{test} : X \mapsto X$  (the attacker uses  $\tau_{test}$  to construct poisoned test images without changing the ground-truth label of the poisoned image). The

attacker is allowed (but not required) to pick  $A$ ,  $\tau_{train}$ , and  $\tau_{test}$  after observing  $D$ . The attacker then poisons the samples in  $A$  to obtain poisoned samples  $P = \{\tau_{train}(a) \mid a \in A\}$ . The threat model places no restrictions on  $\tau_{train}$ , but requires that  $\tau_{test}$  should not affect the predictions of a network trained on  $C$ . The final poisoned training set is  $C \cup P$ .

Let  $\theta$  be the parameters of the network under attack. Given  $m$  fresh test samples  $T$  drawn iid from  $\mathcal{D}$ , the attacker seeks to maximize the *targeted misclassification rate* (TMR):

$$A_{emp}(\theta; T) := \frac{1}{m} \sum_{i=1}^m L(f_{\theta}(x_i), \neg y_i) * L(f_{\theta}(\tau_{test}(x_i)), y_i), \quad (1)$$

i.e., the attack succeeds if it can flip the label of a correctly-classified instance by applying the trigger  $\tau_{test}(\cdot)$  at test time. This metric captures both the “hidden” nature of the backdoor (the first term rewards the attacker only if clean inputs are correctly classified) as well as control upon application of the trigger (the second term rewards the attacker only if poisoned inputs are misclassified).

## 2.2 DEFENSE CAPABILITIES AND OBJECTIVE

The defender is given only the poisoned dataset  $C \cup P$ . In particular,  $\tau_{train}$ ,  $\tau_{test}$ ,  $A$ , and  $C$  are not available to the defender. The defender’s objective is to return a sanitized dataset  $\tilde{D} \subseteq C \cup P$  such that the learned parameters  $\tilde{\theta} := \mathcal{A}(\tilde{D})$  are as close as possible to the ground-truth parameters  $\theta^* := \mathcal{A}(C)$ . Note that  $\theta^*$  is guaranteed to exhibit low targeted misclassification rate—the threat model requires that for fresh  $(x, y)$  drawn from  $\mathcal{D}$ ,  $f_{\theta^*}(\tau_{test}(x)) = y$  with high probability.

## 3 INCOMPATIBILITY AND BACKDOOR ATTACKS

We next define a formal notion of incompatibility which captures the intuition that poisoned data should not improve performance on clean data (and vice versa). One technical challenge is that, in the setting of Section 2.2, the defender has no access to any ground-truth labels. We therefore work with a “self-expansion” property: given a set of data points, we first subsample the data to obtain a smaller training set, then measure how well the learning algorithm generalizes to the full set of data. Then, by leveraging the incompatibility property, we prove that a set that achieves *optimal* expansion is homogeneous, i.e., is composed entirely of either clean or poison data.

### 3.1 SELF-EXPANSION AND COMPATIBILITY

We begin by formally characterizing the self-expanding property of sets, which allows us to measure a notion of generalization without holdout data and independent of the ground truth labels:

**Definition 3.1** (Self-expansion of sets.). *Let  $S$  and  $T$  be sets ( $S$  nonempty), and let  $\alpha \in (0, 1]$  denote the subsampling rate. We define the  $\alpha$ -expansion error of  $S$  given  $T$  as*

$$\epsilon(S|T; \alpha) := \mathbb{E}_{S' \sim S \cup T} [R_{emp}(\mathcal{A}(S'); S)] \quad (2)$$

where the expectation is over both the randomness in  $\mathcal{A}$  and  $S'$ , a random variable that samples a uniformly random  $\alpha$  fraction per class (rounded up) from  $S \cup T$ . When  $T = \emptyset$  we also write  $\epsilon(S; \alpha)$ .

Here  $\alpha$  is a hyperparameter that is typically selected *a priori* on the basis of some domain knowledge (for instance, if one takes  $\alpha = 1$  and  $\mathcal{A}$  trains a deep neural network, then memorization of the training set can occur). A typical value of  $\alpha$  is  $1/4$  or  $1/2$ ; in our ablation studies, we find that our particular application is robust to a wide range of  $\alpha$ .

The self-expansion property measures the ability of the learning algorithm  $\mathcal{A}$  to generalize from a subset of  $S \cup T$  to the empirical distribution of  $S$ . Intuitively, when  $T = \emptyset$ , a smaller expansion error means that the set  $S$  is both “easier” and “more homogeneous” with respect to the learning algorithm, as a random subset is sufficient to learn the contents of  $S$ . When  $T$  is not empty, we expect that the self-expansion error will be lower when  $T$  contains similar data as  $S$  (for instance, if both  $S$  and  $T$  are drawn from the same distribution  $\mathcal{D}$ ).

This observation leads directly to our formal definition of compatibility between sets:

**Definition 3.2** (Compatibility of sets.). *A set  $T$  is  $\alpha$ -compatible with set  $S$  with margin  $\delta \geq 0$  if*

$$\epsilon(S|T; \alpha) + \delta \leq \epsilon(S; \alpha). \quad (3)$$

*Conversely,  $T$  is  $\alpha$ -incompatible with  $S$  if the opposite holds, i.e.,*

$$\epsilon(S; \alpha) + \delta \leq \epsilon(S|T; \alpha). \quad (4)$$

*Furthermore,  $T$  is completely  $\alpha$ -compatible with  $S$  if every subset of  $T$  is  $\alpha$ -compatible with every subset of  $S$ , and the compatibility is strict if  $\delta > 0$  (and similarly for incompatibility).*

In other words,  $T$  is (formally) compatible with  $S$  if  $T$  improves the ability of  $\mathcal{A}$  to generalize to  $S$ .

### 3.2 MODELING BACKDOOR POISONING ATTACKS AS INCOMPATIBLE DATA

We next introduce our formal model of backdoor data poisoning attacks. Recall that our main intuition is that increasing the amount of clean data in the training set should not improve the performance on poisoned data, and vice versa:

**Definition 3.3** (Incompatibility Property). *Let  $C$  and  $P$  be the clean and poisoned data produced by an attacker according to threat model defined in Section 2.1. We say that the attacker satisfies the incompatibility property if  $C$  and  $P$  are mutually completely incompatible. Furthermore if at least one of the incompatibilities between  $C$  and  $P$  is strict, then the attacker satisfies the strict incompatibility property.*

Note that incompatibility here is defined with respect to the learning algorithm  $\mathcal{A}$  as well as the sub-sampling rate  $\alpha$ . We have found that  $\alpha \in [1/4, 1/2]$  works well in practice.

We next present a backdoor attack against linear classifiers which provably satisfies the incompatibility property.

**Theorem 3.4.** *Let the input space be  $X = \mathbb{R}^N$  ( $N > 1$ ). We use the parametric family of functions  $f_{w,b}$  consisting of linear separators given by  $f_{w,b}(x) = \text{sign}(\langle w, x \rangle + b)$  for  $w \in \mathbb{R}^N, b \in \mathbb{R}$ .  $\mathcal{A}$  selects the maximum margin classifier. Then there exists a distribution  $\mathcal{D}$  and perturbation functions  $\tau_{\text{train}}$  and  $\tau_{\text{test}}$ , such that if the adversary poisons  $1/4$  of each class at random, then with high probability over the initial training samples:*

1. *Given the clean dataset,  $\mathcal{A}$  returns parameters with 0 empirical (and population) risk.*
2. *Given the poisoned dataset,  $\mathcal{A}$  returns parameters with a targeted misclassification rate of 1.*
3. *The clean and poisoned data are mutually completely incompatible.*

The proof is deferred to Appendix A. The idea is to construct a dataset such that there exist dimensions in the original, clean feature space that are uncorrelated with the true labels, i.e., consist of pure noise. The backdoor data poisoning attack makes use of these extra dimensions by replacing the noise with a backdoor signal. Although simplified, this setting is analogous to many existing attacks against DNNs. For example, a common perturbation function for backdoor attacks against image classifiers inserts a small synthetic patch on the border of the image, which, by design, is a location that does not affect the original classification task. Hence, the labels for clean and poisoned data depend on disjoint portions of the image.

### 3.3 SEPARATION OF INCOMPATIBLE DATA

We next state a key result that allows us to separate clean and poisoned data satisfying the incompatibility property (proof in Appendix A). The main idea is that, given any set, we can always achieve better self-expansion by removing incompatible data (if it exists).

**Theorem 3.5** (Sets minimizing expansion error are homogeneous.). *Let  $S = A \cup B$  be a set with  $A$  and  $B$  nonempty and mutually completely  $\alpha$ -incompatible. Define*

$$\epsilon^* := \min_{S' \subseteq S} \epsilon(S'; \alpha), \quad (5)$$

*let  $\mathcal{S}^*$  be the collection of subsets of  $S$  that achieve  $\epsilon^*$ . Then for any smallest subset  $S_{\min}^* \in \mathcal{S}^*$ , either  $S_{\min}^* \subseteq A$  or  $S_{\min}^* \subseteq B$ . Furthermore, if at least one of the incompatibilities is strict, then for all  $S^* \in \mathcal{S}^*$  we have either  $S^* \subseteq A$  or  $S^* \subseteq B$ .*

**Algorithm 1** Boosting Homogeneous Sets**Input:** Homogeneous sets  $S_1, \dots, S_N$ , number of samples  $n = \sum_{i=1}^N |S_i|$ , learning algorithm  $\mathcal{A}$ **Output:** Votes  $V_1, \dots, V_N$ 

```

1:  $C_1, \dots, C_N \leftarrow 0$ 
2: for  $i = 1$  to  $N$  do
3:    $\theta_i \leftarrow \mathcal{A}(S_i)$ 
4:   for  $k = 1$  to  $N$  do
5:     if  $\text{LOSS}_{0,1}(\theta_i; S_k) < |S_k|/2$  then
6:        $C_k \leftarrow C_k + |S_i|$ 
7:     end if
8:   end for
9: end for
10: for  $i = 1$  to  $N$  do
11:    $V_i \leftarrow C_i > n/2$ 
12: end for

```

Theorem 3.5 suggests an iterative procedure for separating clean and poisoned data that satisfy the incompatibility property. Namely, at each step  $i$ , identify  $S_{min}^*$  in the current dataset  $D_i$ , then repeat the procedure with  $D_{i+1} = D_i \setminus S_{min}^*$ . The procedure terminates when  $D_{i+1} = \emptyset$ . Assuming the attacker satisfies the incompatibility property, this process partitions the training set into subsets that are guaranteed to contain either entirely clean or entirely poisoned data. If the attacker satisfies strict incompatibility, we can instead take the largest  $S^* \in \mathcal{S}^*$  at each step. The next section leverages this insight to develop a practical defense mechanism against backdoor data poisoning attacks.

## 4 DEFENDING AGAINST BACKDOOR ATTACKS

We next present a tractable defense against backdoor data poisoning attacks under the threat model specified in Section 2 for attackers that satisfy the incompatibility property. In particular, although Theorem 3.5 yields a method of partitioning the dataset into clean and poisoned components, it remains to *identify* which components are clean. Additionally, at each iteration, we need to solve an optimization problem which is intractable in general. The following sections resolve these questions.

### 4.1 IDENTIFICATION USING BOOSTING

We first consider the task of identifying the clean data from a collection of homogeneous (i.e., entirely clean or entirely poisoned) subsets. One idea is to measure the compatibility between each pair of subsets, then take the largest mutually compatible (sub)collection of subsets (under the assumption that the clean data is always compatible with itself). However in general this requires training on each subset multiple times in sequence. We instead propose a simplified boosting algorithm for identifying the clean data which involves training on each subset exactly once. The main idea is to fit a weak learner to each component, then use each weak learner to vote on the other components.

Before we begin, we establish sufficient conditions for the boosting algorithm to succeed:

**Property 4.1** (Compatibility property of disjoint sets). *Let  $C'$  and  $C''$  be any two disjoint sets of clean data, and let  $P'$  be a set of poisoned data. Then*

$$R_{emp}(\mathcal{A}(C'); C'') < 1/2 \leq R_{emp}(\mathcal{A}(C'); P'). \quad (6)$$

The first inequality says that training and testing on disjoint sets of clean data is an improvement over random guessing. The second inequality says that training with clean data then testing on poisoned data is at best equivalent to random guessing; this property is natural in that the threat model already guarantees  $R_{emp}(\mathcal{A}(C); P)$  is large (i.e., close to 1) for *random* poisoned data  $P$ .

Algorithm 1 presents our approach for boosting from homogeneous sets. The subroutine  $\text{LOSS}_{0,1}$  takes a set of parameters and a set  $S$ , and returns the total risk over  $S$  using the zero-one loss. Note that votes are weighted by size. The main result of this section is the correctness of Algorithm 1; the proof is deferred to Appendix A.

**Algorithm 2** Inverse Self-Paced Learning

---

**Input:** training set  $S$ , total iterations  $N$ , annealing schedule  $1 \geq \beta_0 \geq \dots \geq \beta_N = \beta_{\min} > 0$ , expansion  $\alpha \leq 1$ , momentum  $\eta \in [0, 1]$ , learning algorithm  $\mathcal{A}$ , initial parameters  $\theta_0$

**Output:**  $S_N \subseteq S$  such that  $|S_N| = \beta_{\min}|S|$

```

1:  $S_0 \leftarrow S$ 
2:  $L \leftarrow \mathbf{0}$ 
3: for  $t = 1$  to  $N$  do
4:    $S' \leftarrow \text{SAMPLE}(S_{t-1}, \alpha)$ 
5:    $\theta_t \leftarrow \mathcal{A}(S', \theta_{t-1})$ 
6:    $L \leftarrow \eta L + (1 - \eta)R_{\text{emp}}(\theta_t; S)$ 
7:    $S_t \leftarrow \text{TRIM}(L, \beta_t)$ 
8: end for

```

---

**Theorem 4.2** (Identification of clean samples). *Let  $S_1, \dots, S_N$  be a collection of homogeneous subsets containing either entirely clean or entirely poisoned data. Then if the clean and poisoned data satisfy Property 4.1, Algorithm 1 votes  $V_i = \text{True}$  if  $S_i$  is clean (and  $V_i = \text{False}$  otherwise).*

## 4.2 INVERSE SELF-PACED LEARNING

A major question raised by Theorem 3.5 is how to identify the set  $S^*$ . In general, even computing a single self-expansion error of a given set  $S$  is intractable as it involves taking the expectation over all subsets of size  $\alpha|S|$ .

The *Inverse Self-Paced Learning* (ISPL) algorithm presented below solves this intractability problem. Rather than optimizing over all possible subsets of the training data, we instead seek to minimize the expansion error over subsets of fixed size  $\beta|S|$ . The new optimization objective is defined as:

$$S_\beta^* := \arg \min_{S' \subseteq S: |S'| = \beta|S|} \epsilon(S'; \alpha) \quad (7)$$

We alternate between optimizing parameters  $\theta_t$  and the training subset  $S_t$ —given  $S_{t-1}$ , we update  $\theta_t$  using a single subset from  $S_{t-1}$  of size  $\alpha|S_{t-1}|$ . Then we use  $\theta_t$  to compute the loss for each element in  $S$ , and set  $S_t$  to be the  $\beta$  fraction of the samples with the lowest losses. To encourage stability of the learning algorithm, the losses are smoothed by a momentum term  $\eta$ . To encourage more global exploration in the initial stages, we anneal the parameter  $\beta$  from an initial value  $\beta_0$  down to the target value  $\beta_{\min}$ .

Algorithm 2 presents the full algorithm. `SAMPLE` takes a set  $S$  and samples an  $\alpha$  fraction of each class uniformly at random; `TRIM` takes losses  $L$  and returns the  $\beta$  fraction with the lowest loss.

To conclude, we show for certain choices of parameters that Algorithm 2 converges to a local optimum of the following objective over the training set  $S$ :

$$F(\theta_t, S_t; \beta_t) := \sum_{i \in S_t} L(f_{\theta_t}(x_i), y_i) + \max(0, \beta_t|S| - |S_t|) \quad (8)$$

where  $S_t$  is a subset of  $S$  and  $\beta_t$  is decreasing in  $t$  (proof in Appendix A).

**Proposition 4.3.** *Let  $\alpha = 1$  and  $\eta = 0$  in the setting of Algorithm 2, and assume that  $\mathcal{A}$  returns the empirical risk minimizer. Then we have that for each round of the algorithm,  $F(\theta_t, S_t; \beta_t)$  is decreasing in  $t$  and furthermore,  $|F(\theta_t, S_t; \beta_t) - F(\theta_{t+1}, S_{t+1}; \beta_{t+1})| \xrightarrow{t \rightarrow \infty} 0$ .*

## 5 EXPERIMENTAL EVALUATION

We report empirical evaluations of the incompatibility property (Section 5.1) and the proposed defense (Section 5.2). We use the CIFAR-10 dataset (Krizhevsky & Hinton, 2009) for general image recognition, containing 10 classes of 5000 training and 1000 test images each, and the GTSRB dataset (Stallkamp et al., 2012) for traffic sign recognition, containing 43 classes with 26640 training and 12630 test images. The GTSRB training set is highly imbalanced, with classes ranging from 150 to 1500 instances.



Figure 1: Pairs of poisoned (top) and clean (bottom) samples for all datasets, selected for visible triggers. From left to right: CIFAR-10 with CLBD using GAN,  $\ell_2$ , and  $\ell_\infty$  perturbations, DLBD, and WATERMARK attacks; and GTSRB with DLBD and WATERMARK attacks.

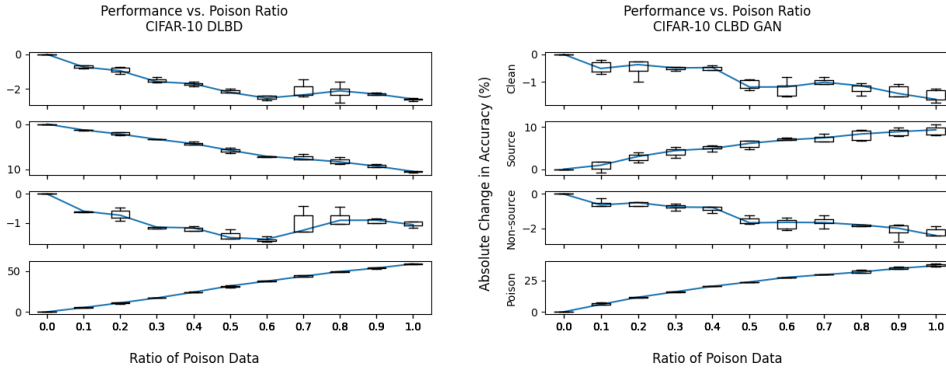


Figure 2: Selected results from incompatibility the experiments on CIFAR-10.

Our experiments use three types of backdoor attacks. Dirty label backdoor (DLBD) uses small patches ranging from a single pixel to a 3x3 checkerboard pattern, using the implementation of Tran et al. (2018). WATERMARK uses 8x8 images such as a copyright sign or a peace sign, following Gao et al. (2019). Both of these attacks insert a patch into a training image from a source class, then change the training label to the target class. The final strategy, clean label backdoor (CLBD), uses the poisoned datasets from Turner et al. (2018), which are only available for CIFAR-10; this attack first strongly perturbs an image of the target class using either GAN,  $\ell_2$ , or  $\ell_\infty$  bounds, then inserts several patches, and does not change the training label. In all cases, the attacker’s objective is to induce the learner to misclassify images as the target class upon application of the patch. Figure 1 presents examples from each dataset. Additional dataset construction details can be found in Appendix B. Full experimental details and additional results, including performance against an adaptive white-box attacker and experiments testing the sensitivity of ISPL to its hyperparameters, are contained in Appendices C and D.

### 5.1 INCOMPATIBILITY BETWEEN CLEAN AND POISONED DATA

We evaluate whether the attacks satisfy the incompatibility property by measuring the gap between  $\epsilon(C; \alpha)$  and  $\epsilon(C|P; \alpha)$  for clean data  $C$  and poisoned data  $P$  using the 3 strategies (DLBD, WATERMARK, CLBD) on CIFAR-10.

Figure 2 presents selected plots for two scenarios: DLBD (e.g., misclassifying patched airplanes as birds), and CLBD using GAN-based perturbations (e.g., misclassifying patched images as airplane). Along the x-axis, we increase the ratio of poisoned to clean data in the source class from 0 to 1. To create the training data, we first sample  $1/8$  of each class in the clean dataset to create  $C$ . For each poison ratio, we sample 5 subsets of poisoned data according to the poison ratio, add it to  $C$ , measure the test accuracies after training at  $\alpha = 1/2$ , then take the mean as the self-expansion error. The entire process is repeated for 5 samples of  $C$  for each poisoned dataset in our evaluations (8 total for DLBD, 5 total for GAN-based CLBD). Since the salient measurement is  $\epsilon(C|P; \alpha) - \epsilon(C; \alpha)$ , we report each metric as an absolute different in accuracy from the unpoisoned case (ratio = 0).

Table 1: Summary of performance for **ISPL+B** across several datasets and poisoning strategies.

	CIFAR-10					GTSRB		totals
	1-to-1	DLBD all-to-1	all-to-all	WATERMARK	CLBD	DLBD	WATERMARK	
$\epsilon = 5$	7 / 8	4 / 4	4 / 4	6 / 8	15 / 15	6 / 8	8 / 8	50 / 55
$\epsilon = 10$	8 / 8	4 / 4	2 / 4	5 / 8	15 / 15	6 / 8	8 / 8	48 / 55
$\epsilon = 20$	7 / 8	4 / 4	2 / 4	1 / 8	11 / 15	5 / 8	6 / 8	36 / 55
totals	22 / 24	12 / 12	8 / 12	12 / 24	41 / 45	17 / 24	22 / 24	134 / 165

The first plot displays the quantity  $\epsilon(C|P; \alpha) - \epsilon(C; \alpha)$  as the size of  $P$  increases. The next two plots separate the test set  $C$  into the source and non-source classes. The final plot shows accuracy on poisoned data. A trendline connects the medians.

Our first observation is that the key quantity,  $\epsilon(C|P; \alpha) - \epsilon(C; \alpha)$ , is negative for all poisoned datasets, which empirically supports our insight that clean and poisoned data are incompatible (or even strictly incompatible), despite the qualitative difference behind the attack mechanisms. The trend in the top plot also indicates that the gap between  $\epsilon(C|P; \alpha)$  and  $\epsilon(C; \alpha)$  increases with the amount of poisoned data. The next two plots show how the gap breaks down over the source and non-source classes. For the DLBD attack, the source class shows a strong negative trend in accuracy as the amount of poison increases, while accuracy on the non-source classes stays largely constant. This fact is consistent with the hypothesis that the poisoned data is impairing the accuracy of the classifier on clean data from the source class (e.g., clean airplanes are getting misclassified as birds).

For the CLBD attack, even though the total clean accuracy decreases, the source class accuracy actually increases as the amount of poison increases. We attribute this phenomenon to the harder poisoned training instances in source class making the classifier more robust on clean instances as well. The decrease in clean accuracy is therefore due to a drop in accuracy among the non-source classes. Because the CLBD attack produces perturbations of the source class toward other classes (thus making the other classes more similar to, e.g., airplanes), this behavior is consistent with the classifier misclassifying clean instances of non-source classes as the source class. These observations are corroborated by the increase in accuracy on poisoned data in both cases, suggesting that the classifier’s mistakes on clean data are correlated with increased accuracy on similar-looking poisoned data. Appendix D contains further discussion and results; violations of incompatibility are rare and small in magnitude.

## 5.2 PERFORMANCE OF PROPOSED DEFENSE

We next evaluate the performance of our proposed defense on the full range of attacks. Each attack is parameterized by  $\epsilon$ , a percentage controlling the amount of the source class that is poisoned in the training set. Most settings use one-to-one attacks (e.g., place a trigger on dogs and mislabel as cats; an  $\epsilon$  percentage of the source class is poisoned), which is the most common setting in the literature (Gu et al., 2019). For the CIFAR-10 DLBD scenario, we additionally use all-to-one (e.g., place a trigger on all non-cats and mislabel as cats; an  $\epsilon/9$  percentage of each non-target class is poisoned) and all-to-all attacks (i.e., place a trigger on any image and mislabel according to a cyclic permutation on classes; an  $\epsilon$  percentage of every class is poisoned).

Table 1 presents a summary of our results. Each cell is of the format "success / total", where total indicates the total number of different scenarios for the attack setting (i.e., different source and target class and trigger combinations), and a run is successful when the defense achieves TMR below 1%. We note that the clean accuracy is around 91% on CIFAR-10 and 94% on GTSRB after running **ISPL+B**, compared to around 93% and 94% when training on the original clean datasets, respectively. These results indicate that our approach succeeds in defending against various backdoor poisoning attacks, particularly for the standard settings of  $\epsilon = 5, 10$  in the literature (Tran et al., 2018), for a small cost in clean accuracy. Appendix D contains the unabridged results.

**Comparison with Existing Approaches.** We also compared the performance of our defense with 3 existing defenses on the CIFAR-10 DLBD (1-to-1) scenario. The plots in Figure 3 display, for  $\epsilon = 5, 10, 20$ , respectively, how many scenarios (out of 8 total) were successfully defended below



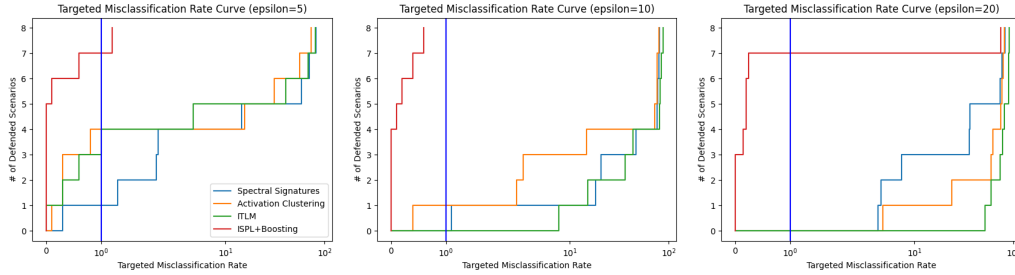


Figure 3: Comparisons with 3 existing baseline defenses on the CIFAR-10 DLBD (1-to-1) scenario.

the TMR along the x-axis. The vertical blue line at 1% corresponds to the definition of success used in Table 1 (i.e., a TMR below 1%). **ISPL+B** outperforms all 3 baselines in terms of reducing the TMR. Table 2 in Appendix D contains detailed results of this experiment for all 4 defenses.

## 6 RELATED WORK

**Compatibility.** Our separation results can be viewed as solutions to a clustering problem, where we exploit weak supervision in the form of (possibly poisoned) class labels. In particular, Balcan et al. (2005) introduce a method called “co-training”, and show that under a similar compatibility property, learners fit independently to two different “views” of the data can supervise each other to improve the joint performance. However, they (and similar works) assume access to a small set of trusted labels not present in our setting and do not consider the case of malicious training data.

**Self-Paced Learning.** Self-Paced learning (SPL) (Kumar et al., 2010) is a type of curriculum learning (CL) (Bengio et al., 2009) that dynamically creates a curriculum by including samples of increasing difficulty based on the losses of the partially trained model. Prior works generally apply SPL to improve convergence on noisy datasets (Meng et al., 2016; Jiang et al., 2018; Zhang et al., 2020). In contrast, ISPL *discards* progressively *easier* samples to identify a subset with good expansion; to the best of our knowledge we are also the first to apply CL ideas to backdoor attacks.

**Backdoor Data Poisoning Defenses.** Many prior works propose methods for defending against backdoor attacks on neural networks. Here we focus on theoretically motivated approaches. One common strategy is to first fit a deep network to the poisoned distribution, then analyze the learned representations. The Activation Clustering defense (Chen et al., 2018) runs k-means clustering ( $k=2$ ) on the activation patterns, then discards the smallest cluster. Tran et al. (2018) propose a defense based on the assumption that clean and poisoned data are separated by their top eigenvalue in the spectrum of the activations. TRIM (Jagielski et al., 2021) (for linear regression) and ITLM (Shen & Sanghavi, 2019) (for generalized linear models) iteratively train on a subset of the data created by removing samples with high loss. However, each iteration removes the same small number of samples, unlike the dynamic resizing in ISPL; both the experiments with ITLM as a baseline and our ablation studies suggest that partitioning by gradual refinement is crucial to the success of our defense. Finally, several works explore the related problem of certifying safety against data poisoning attacks (Steinhardt et al., 2017; Jia et al., 2022); in exchange for the stronger guarantee, these works defend only a small fraction of the dataset, e.g., the current state-of-the-art certifies 16% of CIFAR-10 against 50 poisoned images (Wang et al., 2022).

## 7 CONCLUSION

Backdoor data poisoning attacks on deep neural networks are an emerging class of threats in the growing landscape of deployed machine learning applications. We present a new defense against backdoor attacks based on a novel incompatibility property of the interaction between clean and poisoned data and the training algorithm. The experimental results show that previous dirty-label and clean-label backdoor attacks produce poisoned datasets that exhibit behavior consistent with the

incompatibility property. The results also highlight the effectiveness of our technique in defending against three backdoor poisoning attacks while preserving clean accuracy.

## REFERENCES

- Yossi Adi, Carsten Baum, Moustapha Cisse, Benny Pinkas, and Joseph Keshet. Turning your weakness into a strength: Watermarking deep neural networks by backdooring. In *27th {USENIX} Security Symposium ({USENIX} Security 18)*, pp. 1615–1631, 2018.
- Maria-Florina Balcan, Avrim Blum, and Ke Yang. Co-training and expansion: Towards bridging theory and practice. *Advances in neural information processing systems*, 17:89–96, 2005.
- Yoshua Bengio, Jérôme Louradour, Ronan Collobert, and Jason Weston. Curriculum learning. In *Proceedings of the 26th annual international conference on machine learning*, pp. 41–48, 2009.
- Bryant Chen, Wilka Carvalho, Nathalie Baracaldo, Heiko Ludwig, Benjamin Edwards, Taesung Lee, Ian Molloy, and Biplav Srivastava. Detecting backdoor attacks on deep neural networks by activation clustering. *arXiv preprint arXiv:1811.03728*, 2018.
- Xinyun Chen, Chang Liu, Bo Li, Kimberly Lu, and Dawn Song. Targeted backdoor attacks on deep learning systems using data poisoning. *arXiv preprint arXiv:1712.05526*, 2017.
- Yansong Gao, Change Xu, Derui Wang, Shiping Chen, Damith C. Ranasinghe, and Surya Nepal. Strip: A defence against trojan attacks on deep neural networks. In *Proceedings of the 35th Annual Computer Security Applications Conference, ACSAC ’19*, pp. 113–125, New York, NY, USA, 2019. Association for Computing Machinery. ISBN 9781450376280. doi: 10.1145/3359789.3359790. URL <https://doi.org/10.1145/3359789.3359790>.
- Tianyu Gu, Brendan Dolan-Gavitt, and Siddharth Garg. Badnets: Identifying vulnerabilities in the machine learning model supply chain. *arXiv preprint arXiv:1708.06733v1*, 2017.
- Tianyu Gu, Brendan Dolan-Gavitt, and Siddharth Garg. Badnets: Identifying vulnerabilities in the machine learning model supply chain. *arXiv preprint arXiv:1708.06733*, 2019.
- Kaiming He, Xiangyu Zhang, Shaoqing Ren, and Jian Sun. Deep residual learning for image recognition. In *Proceedings of the IEEE conference on computer vision and pattern recognition*, pp. 770–778, 2016a.
- Kaiming He, Xiangyu Zhang, Shaoqing Ren, and Jian Sun. Identity mappings in deep residual networks. *arXiv preprint arXiv:1603.05027*, 2016b.
- Matthew Jagielski, Alina Oprea, Battista Biggio, Chang Liu, Cristina Nita-Rotaru, and Bo Li. Manipulating machine learning: Poisoning attacks and countermeasures for regression learning. *arXiv preprint arXiv:1804.00308*, 2021.
- Jinyuan Jia, Yupei Liu, Xiaoyu Cao, and Neil Zhenqiang Gong. Certified robustness of nearest neighbors against data poisoning and backdoor attacks. *AAAI*, 2022.
- Lu Jiang, Zhengyuan Zhou, Thomas Leung, Li-Jia Li, and Li Fei-Fei. Mentornet: Learning data-driven curriculum for very deep neural networks on corrupted labels. In *International Conference on Machine Learning*, pp. 2304–2313. PMLR, 2018.
- Alex Krizhevsky and Geoffrey Hinton. Learning multiple layers of features from tiny images. Technical Report 0, University of Toronto, Toronto, Ontario, 2009.
- M Kumar, Benjamin Packer, and Daphne Koller. Self-paced learning for latent variable models. *Advances in neural information processing systems*, 23:1189–1197, 2010.
- Alexey Kurakin, Ian Goodfellow, and Samy Bengio. Adversarial examples in the physical world. *arXiv preprint arXiv:1607.02533*, 2016.
- Aleksander Madry, Aleksandar Makelov, Ludwig Schmidt, Dimitris Tsipras, and Adrian Vladu. Towards deep learning models resistant to adversarial attacks. *arXiv preprint arXiv:1706.06083*, 2017.

- Deyu Meng, Qian Zhao, and Lu Jiang. What objective does self-paced learning indeed optimize? *arXiv preprint arXiv:1511.06049*, 2016.
- Maria-Irina Nicolae, Mathieu Sinn, Minh Ngoc Tran, Beat Buesser, Ambrish Rawat, Martin Wistuba, Valentina Zantedeschi, Nathalie Baracaldo, Bryant Chen, Heiko Ludwig, Ian M. Molloy, and Ben Edwards. Adversarial robustness toolbox v1.0.0. *arXiv preprint arXiv:1807.01069*, 2019.
- Avi Schwarzschild, Micah Goldblum, Arjun Gupta, John P Dickerson, and Tom Goldstein. Just how toxic is data poisoning? a unified benchmark for backdoor and data poisoning attacks, 2021.
- Yanyao Shen and Sujay Sanghavi. Learning with bad training data via iterative trimmed loss minimization. *arXiv preprint arXiv:1810.11874*, 2019.
- J. Stallkamp, M. Schlipsing, J. Salmen, and C. Igel. Man vs. computer: Benchmarking machine learning algorithms for traffic sign recognition. *Neural Networks*, 32:323–332, 2012. ISSN 0893-6080. doi: <https://doi.org/10.1016/j.neunet.2012.02.016>. URL <https://www.sciencedirect.com/science/article/pii/S0893608012000457>. Selected Papers from IJCNN 2011.
- Jacob Steinhardt, Pang Wei W Koh, and Percy S Liang. Certified defenses for data poisoning attacks. *Advances in neural information processing systems*, 30, 2017.
- Brandon Tran, Jerry Li, and Aleksander Madry. Spectral signatures in backdoor attacks. *arXiv preprint arXiv:1811.00636*, 2018.
- Alexander Turner, Dimitris Tsipras, and Aleksander Madry. Clean-label backdoor attacks. 2018.
- Wenxiao Wang, Alexander J Levine, and Soheil Feizi. Improved certified defenses against data poisoning with (deterministic) finite aggregation. In *International Conference on Machine Learning*, pp. 22769–22783. PMLR, 2022.
- Xuchao Zhang, Xian Wu, Fanglan Chen, Liang Zhao, and Chang-Tien Lu. Self-paced robust learning for leveraging clean labels in noisy data. In *Proceedings of the AAAI Conference on Artificial Intelligence*, volume 34, pp. 6853–6860, 2020.

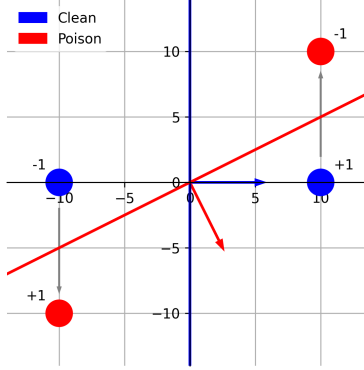


Figure 4: The construction in two dimensions used in our proof of Theorem 3.4. The balls depict the support of the clean training distribution (blue) and the poisoned data (red). The perturbation function  $\tau$  is shown by the grey arrows. The lines are the ground truth maximum margin classifier (blue) and the maximum margin classifier when training with a mixture of clean and poisoned data (red). The red and blue arrows point in the direction of half-plane labelled by the corresponding classifier as the positive class.

## A DEFERRED PROOFS AND ADDITIONAL THEORETICAL RESULTS

*Proof of Theorem 3.4.* First we give a construction when the dimension  $N = 2$ . We define the training distribution as  $\mathcal{D} = (\mathcal{D}_+ + \mathcal{D}_-)/2$ , where  $\mathcal{D}_+$  and  $\mathcal{D}_-$  are both distributed arbitrarily within a ball of radius 1 (e.g., as a truncated Gaussian);  $\mathcal{D}_+$  is centered at  $(10, 0)$  with labels  $+1$  and  $\mathcal{D}_-$  is centered at  $(-10, 0)$  with labels  $-1$ . The adversary chooses the perturbation function  $\tau$  which flips the label during training and sets the last entry to be 10 if the original label was  $+1$ , and  $-10$  if the original label was  $-1$ . Note that  $\tau$  is bounded in the sense that as  $N \rightarrow \infty$ , the (expected) magnitude of a data point is  $O(\sqrt{N})$  while the magnitude of the perturbation is  $O(1)$ . Figure 4 depicts the construction.

Clearly, one sample from each clean class is sufficient to learn a maximum margin classifier (MMC) achieving zero population risk, i.e., the MMC will be close to  $w = (1, 0)$ ,  $b = 0$ .

Next, we show that the attacker succeeds under the threat model in Section 2. Recall that the attacker selects  $1/4$  of the positive samples and  $1/4$  of the negative samples to poison. Given a poisoned dataset containing at least one example of each class (both clean and poisoned), the classifier given by  $w = (1, -2)$ ,  $b = 0$  achieves perfect accuracy on both the clean data and the poisoned data, and hence the MMC also has a poison misclassification rate of 1.

We now show that this setup satisfies the incompatibility property defined in Section 3.2. We begin by showing that the poisoned data is not compatible with the clean data. Let  $C$  be any set of clean data, and let  $P$  be any set of poisoned data. We have two cases. First, if  $C$  contains samples of both classes, then by definition, any subset  $C'$  of  $C$  in the measurement of the self-expansion error will also include at least one sample of each clean class. Hence, the MMC learned from  $C'$  will be close to  $w = (1, 0)$ ,  $b = 0$ , which achieves perfect accuracy on all clean data. On the other hand, if  $C$  contains only samples of the positive class, the MMC is  $w = (0, 0)$ ,  $b = +1$ , and again all samples in  $C$  are correctly classified. The same argument works when  $C$  contains only samples from the negative class. Thus, in neither case can poisoned data improve the self-expansion error of  $C$ .

As the exact same line of reasoning holds for proving incompatibility of clean data with respect to poisoned data, we omit the proof. Therefore the clean and poisoned data are mutually completely incompatible.

To generalize this to  $N > 2$ , we can simply embed  $\mathcal{D}$  in the first two dimensions of the space. The entire construction can also be scaled then translated and rotated without affecting any of the conclusions.  $\square$

Before moving on to the proof of Theorem 3.5, we first prove a useful lemma:

**Lemma A.1.** *Let  $A$  and  $B$  be arbitrary sets, and define  $S = A \cup B$ . Then for all  $\alpha$ ,*

$$|S|\epsilon(S; \alpha) = |A|\epsilon(A|B; \alpha) + |B|\epsilon(B|A; \alpha) \quad (9)$$

*with the convention that  $\epsilon(\emptyset|T; \alpha) = 0$  for all  $T$  and  $\alpha$ .*

*Proof.* Notice that all the expansion errors sample from the same training set  $S = A \cup B$ . The lemma then follows from the linearity of the unnormalized empirical risk in the test set, i.e.,

$$|S|\epsilon(S; \alpha) = |S|\mathbb{E}_{S' \sim S} [R_{emp}(\mathcal{A}(S'); S)] \quad (10)$$

$$= |S|\mathbb{E}_{S' \sim S} \left[ |S|^{-1} \sum_{(x_i, y_i) \in S} L(f_{\mathcal{A}(S')}(x_i), y_i) \right] \quad (11)$$

$$= \mathbb{E}_{S' \sim S} \left[ \sum_{(x_i, y_i) \in A} L(f_{\mathcal{A}(S')}(x_i), y_i) + \sum_{(x_i, y_i) \in B} L(f_{\mathcal{A}(S')}(x_i), y_i) \right] \quad (12)$$

$$= \mathbb{E}_{S' \sim S} [ |A| R_{emp}(\mathcal{A}(S'); A) ] + \mathbb{E}_{S' \sim S} [ |B| R_{emp}(\mathcal{A}(S'); B) ] \quad (13)$$

$$= |A|\epsilon(A|B; \alpha) + |B|\epsilon(B|A; \alpha), \quad (14)$$

as claimed.  $\square$

*Proof of Theorem 3.5.* Assume first that the incompatibility is not strict. Define  $U = S_{min}^* \cap A$  and  $V = S_{min}^* \cap B$ . From Lemma A.1, we have that

$$|S_{min}^*|\epsilon^* = |U|\epsilon(U|V; \alpha) + |V|\epsilon(V|U; \alpha). \quad (15)$$

Applying now the definition of incompatibility gives

$$|S_{min}^*|\epsilon^* \geq |U|\epsilon(U; \alpha) + |V|\epsilon(V; \alpha). \quad (16)$$

As  $|U| + |V| = |S_{min}^*|$ , it follows that at least one of  $\epsilon(U; \alpha)$  or  $\epsilon(V; \alpha)$  is at most  $\epsilon^*$ , which contradicts the optimality of  $S_{min}^*$  (as it was assumed to be a smallest set achieving  $\epsilon^*$ ).

Now we consider the case when at least one of the incompatibilities is strict. Let  $S^*$  be any set in  $S^*$ . Using the definition of strict incompatibility, we get that

$$|S^*|\epsilon^* > |U|\epsilon(U; \alpha) + |V|\epsilon(V; \alpha). \quad (17)$$

Hence, at least one of  $\epsilon(U; \alpha)$  or  $\epsilon(V; \alpha)$  is strictly less than  $\epsilon^*$ , which again contradicts the optimality of  $S^*$ .  $\square$

*Proof of Theorem 4.2.* Let  $S_i$  and  $S_j$  be a clean component and poison component, respectively. By the second inequality in Property 4.1, we have that  $R_{emp}(\mathcal{A}(S_i); S_j) \geq 1/2$ . Thus  $S_i$  votes False on  $S_j$ . Conversely, if both  $S_i$  and  $S_j$  are a clean components, then  $R_{emp}(\mathcal{A}(S_i); S_j) < 1/2$ , so  $S_i$  votes True on  $S_j$ . Putting these together and using the fact that at least half of the data is clean, we find that the poisoned components have weighted vote strictly less than  $|S|/2$ , while the clean components have weighted vote strictly greater than  $|S|/2$ . As all the clean components vote correctly, using the weighted majority correctly identifies all the clean and poisoned components as claimed.  $\square$

*Proof of Proposition 4.3.* Recall that  $\alpha = 1$  and  $\eta = 0$ . We prove the statement in two steps.

First, we show that

$$F(\theta_{t+1}, S_t; \beta_t) \leq F(\theta_t, S_t; \beta_t) \quad (18)$$

The inequality follows from the optimization on Line 5 in Algorithm 2, which sets  $\theta_{t+1}$  to the empirical risk minimizer of the set  $S_t$ .

Next, we claim that

$$F(\theta_{t+1}, S_{t+1}; \beta_{t+1}) \leq F(\theta_{t+1}, S_t; \beta_t) \quad (19)$$

Since  $|L(\cdot, \cdot)| \leq 1$ , the optimal size of the set  $S_t$  is  $|S_t| = \beta_t |S|$ . Since  $\beta_t$  is decreasing, we have that  $|S_{t+1}| \leq |S_t|$ . Thus the number of elements in the trimmed empirical loss is non-increasing (Line 7, Algorithm 2).

Combining the two inequalities shows that the objective function is decreasing in  $t$ . Since  $F(\theta_t, S_t; \beta_t)$  is a decreasing sequence bounded from below by zero, the monotone convergence theorem gives the second result.  $\square$

## B DATASET CONSTRUCTION DETAILS

Our implementation of the 1-to-1 dirty label backdoor (DLBD) adversary follows the threat model described in Gu et al. (2017). For evaluation, we use the same dataset (CIFAR-10 (Krizhevsky & Hinton, 2009)) and setup for our experiments as the Spectral Signatures work (Tran et al., 2018). Each scenario has a single source and target class, and we use the same (source, target) pairs as in Tran et al. (2018): (airplane, bird), (automobile, cat), (bird, dog), (cat, dog), (cat, horse), (horse, deer), (ship, frog), (truck, bird).

The perturbation function  $\tau$  overlays a small pattern on the image at a fixed location. All patterns fit within a 3x3 pixel box. To generate a perturbation, we choose a shape (L-shape, X-shape, or pixel) uniformly at random. The (x,y) coordinates of the perturbation are randomly selected to guarantee that the entire shape is visible before data augmentation (e.g., the pixel-based perturbation can be placed anywhere within the 32x32 image, but the X-shape is larger and so must be centered in a 30x30 region, one pixel away from the border). The color of the perturbation is also selected uniformly at random, with each of the (R,G,B) coordinates ranging from 0 to 255. Finally, we randomly select an  $\epsilon = 5, 10, 20\%$  percentage of the source class, apply the perturbation by replacing the pixels in the corresponding locations with the selected shape and color, then relabel the poisoned images as the target class. For the all-to-1 case, for a given target class, we poison an equal proportion of every non-target class such that the total amount of poison is  $\epsilon$  times the size of the source class. For the all-to-all case, we select a cyclic permutation of the classes, then poison a  $\epsilon$  percentage of each class.

The construction of the WATERMARK dataset is the same, except that we instead use 8x8 images in the upper left depicting: a peace sign, the letter A, 3 bullet holes, or a colorful patch, taken from the Nicolae et al. (2019).

For the CLBD dataset, we used the official datasets provided by Turner et al. (2018). There are three datasets in total, one for each perturbation type:  $\ell_2$ ,  $\ell_\infty$ , and GAN. For the  $\ell_2$  and  $\ell_\infty$ -based attacks, the images are perturbed to maximize the loss with respect to a reference model trained on clean data; the perturbation size is bounded by the respective norm. For the GAN-based attack, a perceptually similar target image in another class is identified using the latent space of the GAN, and the perturbed image is an interpolation of the original and target images in the latent space. In all three cases, a 3x3 checkerboard patch is then placed in each of the 4 corners of the image. The label of the image is not changed. At test time, only the checkerboard patches are placed on the image. We refer the reader to Turner et al. (2018) for more details.

For the GTSRB dataset, we use the same construction of the DLBD and WATERMARK attacks on CIFAR-10. However, as the CLBD dataset was only created for the CIFAR-10 dataset, we did not evaluate the CLBD attack on GTSRB.

## C DEFENSE SETUPS AND HYPERPARAMETERS

**ISPL + Boosting (this work).** For our defense, we use the set of hyperparameters described here unless otherwise noted. For CIFAR-10, we run 8 rounds of ISPL, each of which returns a component

consisting of roughly 12% of the total samples. For GTSRB, we run 4 rounds of ISPL so that each component contains 24% of the total samples. Let  $p$  be the target percentage of samples over the remaining samples (e.g., for CIFAR-10  $p \approx 1/(8 - i + 1)$  in the  $i^{th}$  iteration). Then the number of iterations  $N$  is set to  $2 + \min(3, 1/p)$ .  $\beta$  starts at  $3 * p$  in the first iteration, then drops linearly to its final value of  $p$  over the next 2 iterations. When trimming the training set, we also additionally include the top  $p/2$  samples per class to prevent the network from collapsing to a trivial solution. For the learning procedure  $\mathcal{A}$ , we use standard SGD, trained for 4 epochs per iteration, with a warm-up in the first iteration of 8 epochs. The expansion factor  $\alpha$  is set to  $1/4$ , and the momentum factor  $\eta$  is set to 0.9.

We run ISPL 3 times to generate 24 weak learners. For the boosting framework, each weak learner is trained for 40 epochs on its respective subset, then votes on a per-sample basis. The sample is preserved if the modal vote equals the given label, with ties broken randomly, or the sample is in the lower half of its class by loss.

For CIFAR-10, we also include a final self-training step by training a fresh model for 100 epochs on the recovered samples. The main idea is that a model fit to the full “clean” training data can be used to test the excluded training data, thereby recovering additional consistent data which may have been originally excluded because the weak learners were fit to a small subset of data for fewer epochs. However, it may take several repetitions of training a model from scratch before this self-training process no longer identifies new samples to recover. Therefore, we use a simple self-paced learning algorithm to dynamically adjust the samples during training to limit the self-training to a single iteration. More explicitly, we start with the “clean” samples as returned by the boosting framework. Every 5 epochs, we update the training set to be the samples whose labels agree with the model’s current predictions. Due to the relative frequency with which we resample the training set, we smooth the predictions by a momentum factor of 0.8 so that the training process is less noisy. The samples used for training in the last epoch are returned as the defended dataset. In our experiments, this process decreases the false positive rate (and thus increases the clean accuracy) but does not materially affect the false negative rate (nor the targeted misclassification rate). We did not use self-training for GTSRB as we found the clean accuracy was sufficiently high.

**Spectral Signatures.** We use the official implementation of the Spectral Signatures (SS) defense (Tran et al., 2018) by the authors, available on Github, except that we replace the training procedure with PyTorch (instead of Tensorflow 1.x as in the authors’ original implementation). The authors suggest removing 1.5 times the maximum expected amount of poison from each class for the defense. We remove 20% of each class for  $\epsilon = 5, 10\%$  (to match the procedure in their paper) and 30% of each class for  $\epsilon = 20\%$ . In selecting the layer for the activations, we use the input to the third block of the third layer of the ResNet32 architecture (taken from the SS defense authors’ public implementation). In selecting the layer for the activations, we use the input to the first block of the four layer of the PreActResNet18 architecture (which was found empirically to remove the most poison on the first set of scenarios). We note that the authors indicate the defense should be fairly successful at any of the later layers of the network.

**Iterative Trimmed Loss Minimization.** The Iterative Trimmed Loss Minimization (ITLM) defense (Shen & Sanghavi, 2019) consists of an iterative procedure. Given a setting  $0 < \alpha \leq 1$ , one first trains a model for a number of epochs. Then the  $\alpha$  fraction of samples with the lowest loss are retained for the next iteration. This process is repeated several times, with a fresh model beginning each iteration. The defended dataset is the  $\alpha$  fraction of samples with the lowest loss after the last iteration. For the backdoor data poisoning experiments on CIFAR-10, the authors use 80 epochs for the first round of training, then 40 epochs thereafter; they also set  $\alpha = 98\%$  for  $\epsilon = 5\%$ , and do not test at other values of  $\epsilon$ . We use the same settings, and scale  $\alpha$  linearly with  $\epsilon$ , i.e.,  $\alpha = 96\%$  for  $\epsilon = 10\%$  and  $\alpha = 92\%$  for  $\epsilon = 20\%$ .

**Activation Clustering.** The Activation Clustering (AC) defense (Chen et al., 2018) has an actively maintained official implementation in the Adversarial Robustness Toolbox (ART) (Nicolae et al., 2019), an open-source collection of tools for security in machine learning. We use the official implementation with the default parameters values in ART v1.6.2. In selecting the layer for the activations, we used the same layers as for Spectral Signatures.

**Models.** For the ResNet32 (He et al., 2016a) model, we use vanilla SGD with learning rate 0.1, momentum 0.9, and weight decay  $1e-4$ . For the final dataset, we train for 100 epochs (unless otherwise noted) and drop the learning rate by 10 at epochs 100 and 150. Using these parameters, we achieve around 94.5% accuracy on GTSRB when trained and tested with clean data.

For the PreActResNet18 (He et al., 2016b) model, We use vanilla SGD with learning rate 0.02, momentum 0.9, and weight decay  $5e-4$ . For the final dataset, we train for 100 epochs (unless otherwise noted) and drop the learning rate by 10 at epochs 100, 150, and 180. Using these parameters, we achieve around 93.0% accuracy on CIFAR-10 when trained and tested with clean data.



## D ADDITIONAL EXPERIMENTAL RESULTS

This section contains additional experimental results to complement the main text. Section D.1 expands upon the empirical evaluations of the compatibility property from Section 5.1. Section D.2 reports comprehensive results from the evaluations of the **ISPL+B** defense reported in Section 5.2. Section D.2 also includes a detailed breakdown of the performance for the three defenses (Spectral Signatures, Activation Clustering, and Iterative Trimmed Loss Minimization) we use as baselines in our comparisons. Section D.2.1 evaluates our defense against an adaptive attack that is given white-box access to the ISPL subroutine, and selects which elements to poison based on the behavior of ISPL on clean data. Our results show that **ISPL+B** maintains excellent performance even in this setting, defending against 20/24 scenarios in the adaptive setting. Section D.2.2 reports results for the CIFAR-10 DLBD attack after training for 200 epochs on both the PreActResNet18 and ResNet32 architectures, to test the robustness of our results to the training setup. Finally, to evaluate the sensitivity of ISPL to the main hyperparameters  $\alpha$  and  $\beta$ , Section D.2.3 compares the performance of ISPL on a selection of attack scenarios across a range of  $\alpha$  and  $\beta$ . Our main finding is that performance remains high for a range of choices of  $\alpha$  and  $\beta$ .

All results reported use the median over 3 random seeds, unless otherwise noted.

### D.1 INCOMPATIBILITY EVALUATION

Figures 5-9 displays aggregated results of the empirical study of incompatibility for the CLBD, DLBD, and WATERMARK attacks on CIFAR-10. Plots on the left side measure the compatibility of poisoned with clean data (i.e.,  $\epsilon(C; \alpha) - \epsilon(C|P; \alpha)$ ) and plots on the right side measure the compatibility of clean with poisoned data (i.e.,  $\epsilon(P; \alpha) - \epsilon(P|C; \alpha)$ ).

In all cases, the trend in the first plot is decreasing, which suggests that the gap increases in magnitude as the size of the incompatible data grows. Additionally, the clean label scenarios all exhibit the behavior that the source class accuracy increases as the amount of poison (and poisoned accuracy) increases, while the non-source accuracy drops. These attacks share the characteristic that the poisoned data are “harder” versions of the source class in the sense that they are perturbed toward instances of other classes. In the case of the GAN-based attack, the perturbations occur in the latent space of a GAN trained on clean data (e.g., the attacker identifies a bird and an airplane that are close in the latent space, linearly interpolates the latent representation of the airplane toward the latent representation of the bird, then uses the generative network to convert the perturbed representation into an image of a “bird-like airplane”). In the case of the  $\ell_2$  and  $\ell_\infty$  bounds, the attacker uses the Projected Gradient Descent (PGD) algorithm commonly used for adversarial training (Kurakin et al., 2016; Madry et al., 2017) to identify an image within a norm-bounded neighborhood of the original image that maximizes the loss of a trained network, i.e., the perturbed image is close in pixel-space to the original image, but was misclassified by the trained network as a different class. Hence, the simultaneous increase in source class accuracy and decrease in non-source class accuracies can be attributed to a similar mechanism for all the clean label cases.

Conversely, when measuring the compatibility of poisoned data with clean data (plots on the left) for the DLBD and WATERMARK attacks, we see that, as the amount of poisoned data increases, the source class accuracy drops. The implication is that the poisoned data causes the classifier to misclassify clean data by presenting similar (both quantitatively in terms of the distance between the poisoned and clean distributions, as well as perceptually in most settings) instances of clean source data that are mislabelled as the target class, thus complicating the learning of the clean source class.

However, when measuring the compatibility of clean data with respect to poisoned data (plots on the right) for the DLBD and WATERMARK attacks, the source class accuracy actually increases (as in the clean label case). One explanation is that training with examples of clean instances from the source class improves the ability of the classifier to identify *possibly* poisoned images, hence increasing the accuracy on actual poisoned instances as well.

Finally, Figures 10-14 plot the scenarios individually. We note that incompatibility holds generally across the range of scenarios, with only small deviations to the contrary.

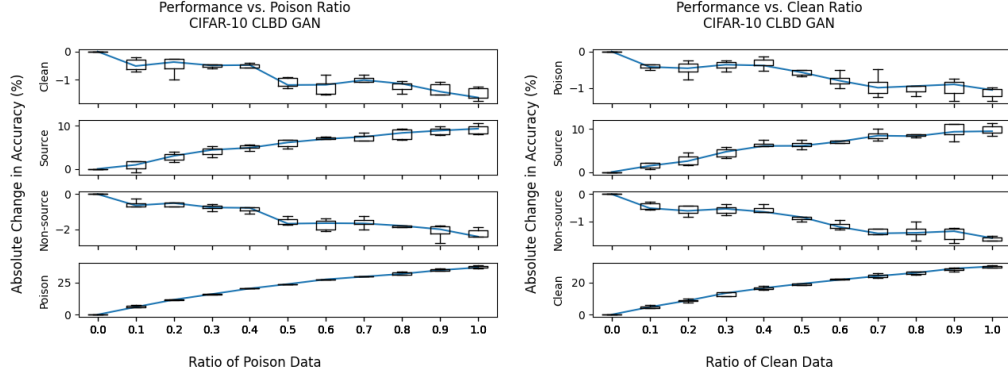
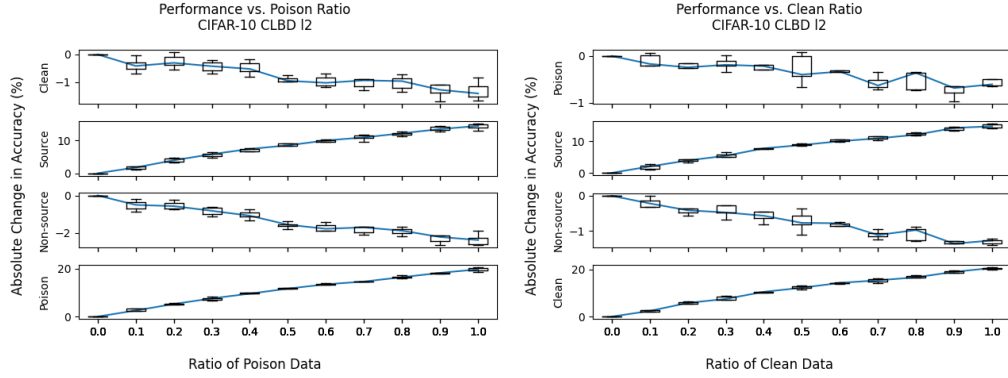
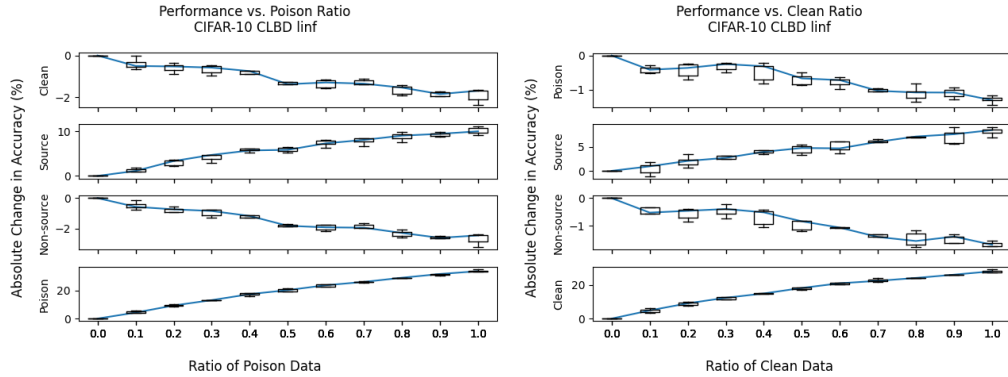


Figure 5: Aggregated compatibility results for the GAN-based CLBD attack on CIFAR-10.

Figure 6: Aggregated compatibility results for the  $\ell_2$ -based CLBD attack on CIFAR-10.Figure 7: Aggregated compatibility results for the  $\ell_\infty$ -based CLBD attack on CIFAR-10.

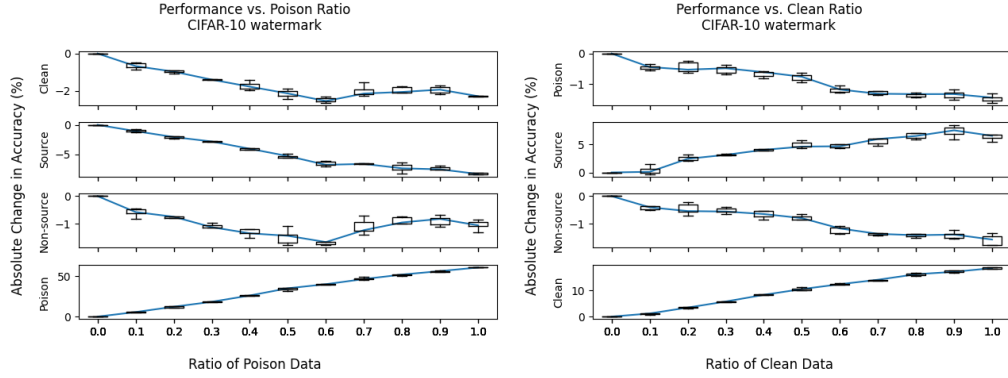


Figure 8: Aggregated compatibility results for the WATERMARK attack on CIFAR-10.

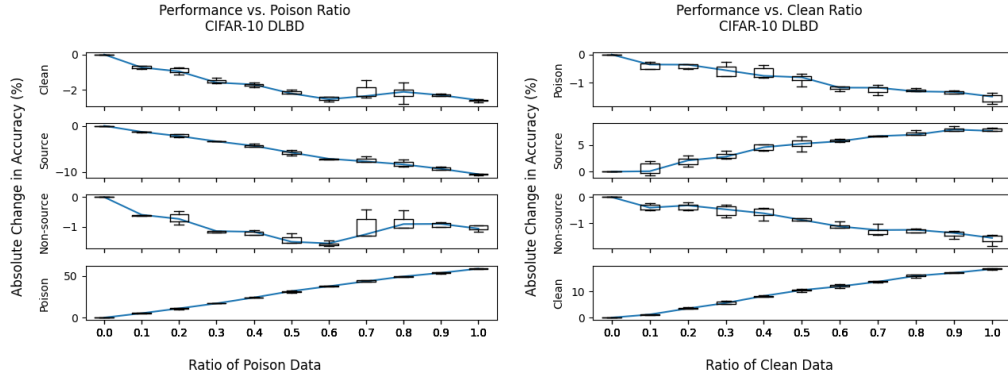


Figure 9: Aggregated compatibility results for the DLBD attack on CIFAR-10.

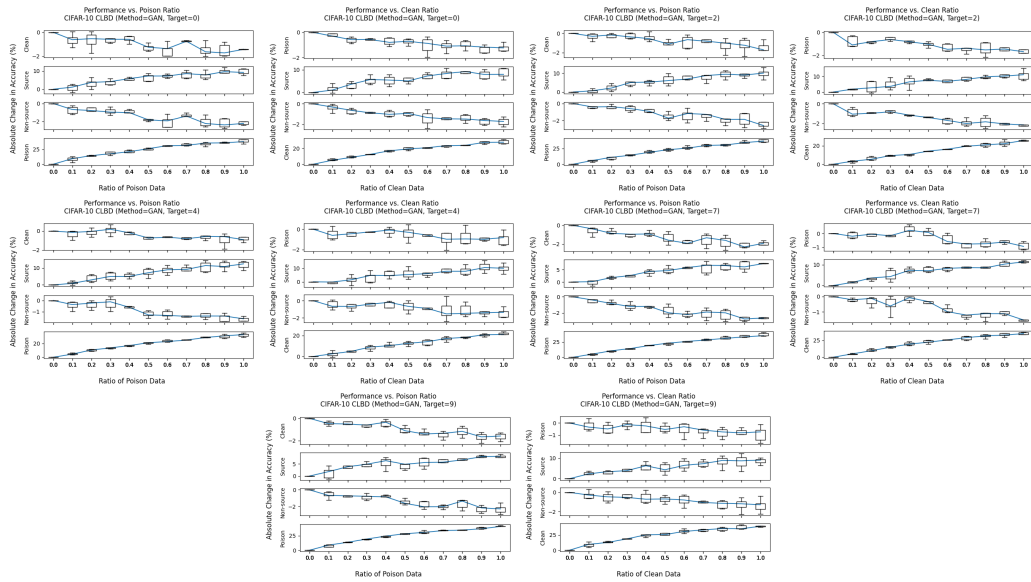
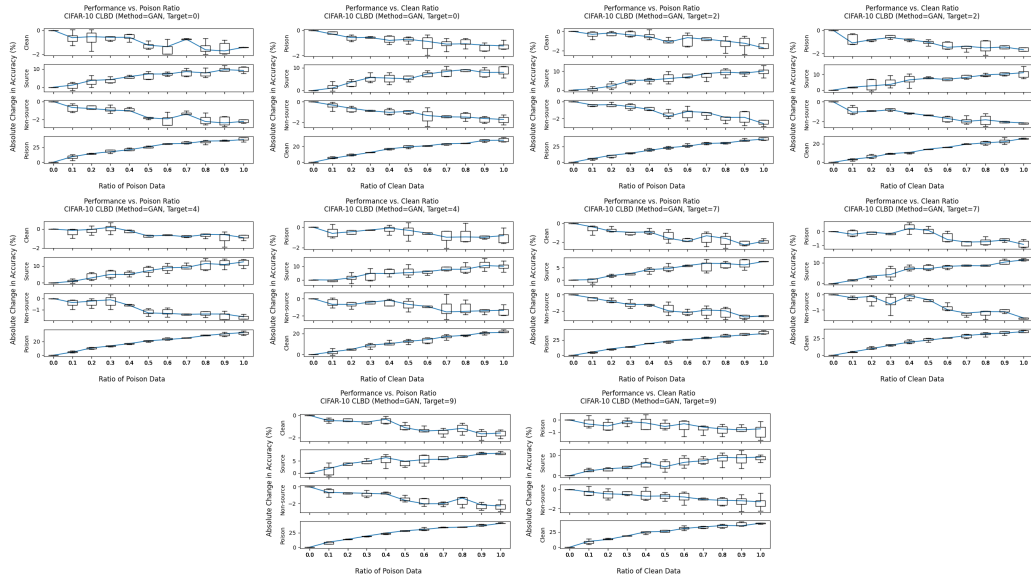
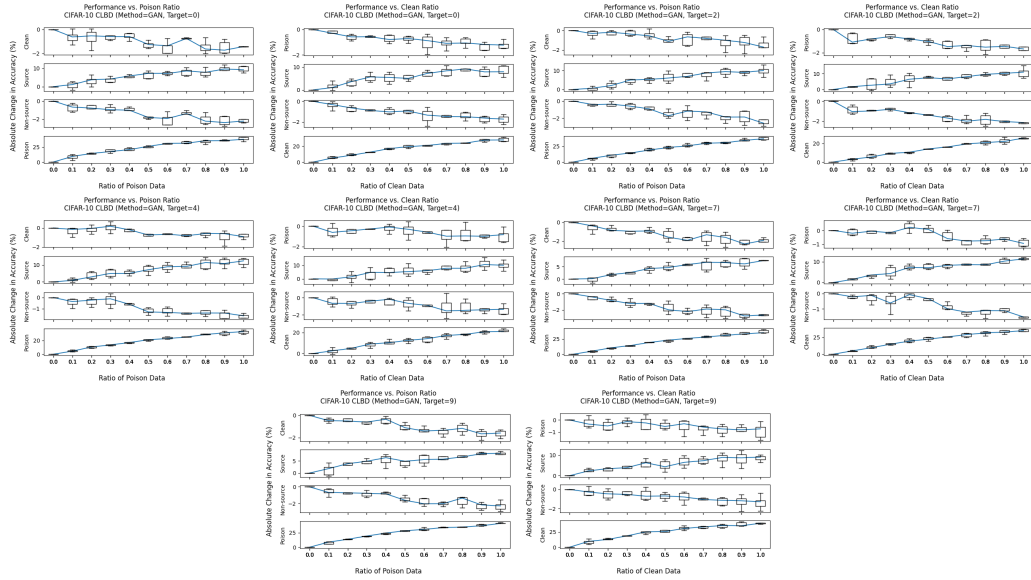


Figure 10: Full compatibility results for the GAN-based CLBD attack on CIFAR-10.

Figure 11: Full compatibility results for the  $\ell_2$ -based CLBD attack on CIFAR-10.Figure 12: Full compatibility results for the  $\ell_\infty$ -based CLBD attack on CIFAR-10.

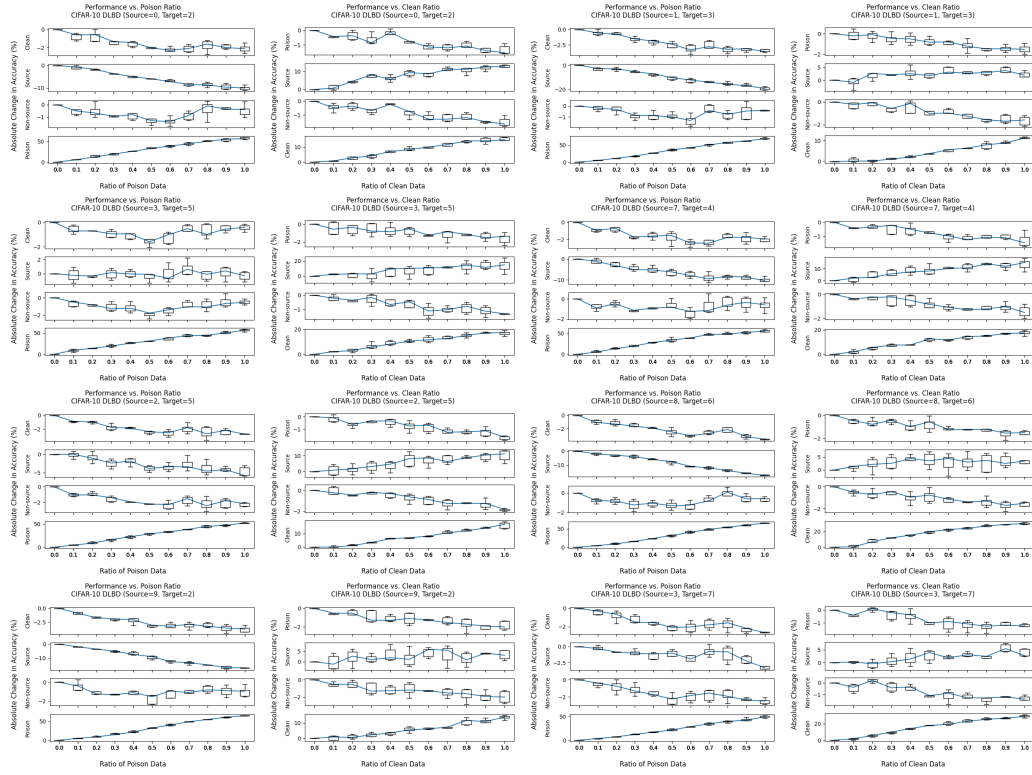


Figure 13: Full compatibility results for the DLBD attack on CIFAR-10.

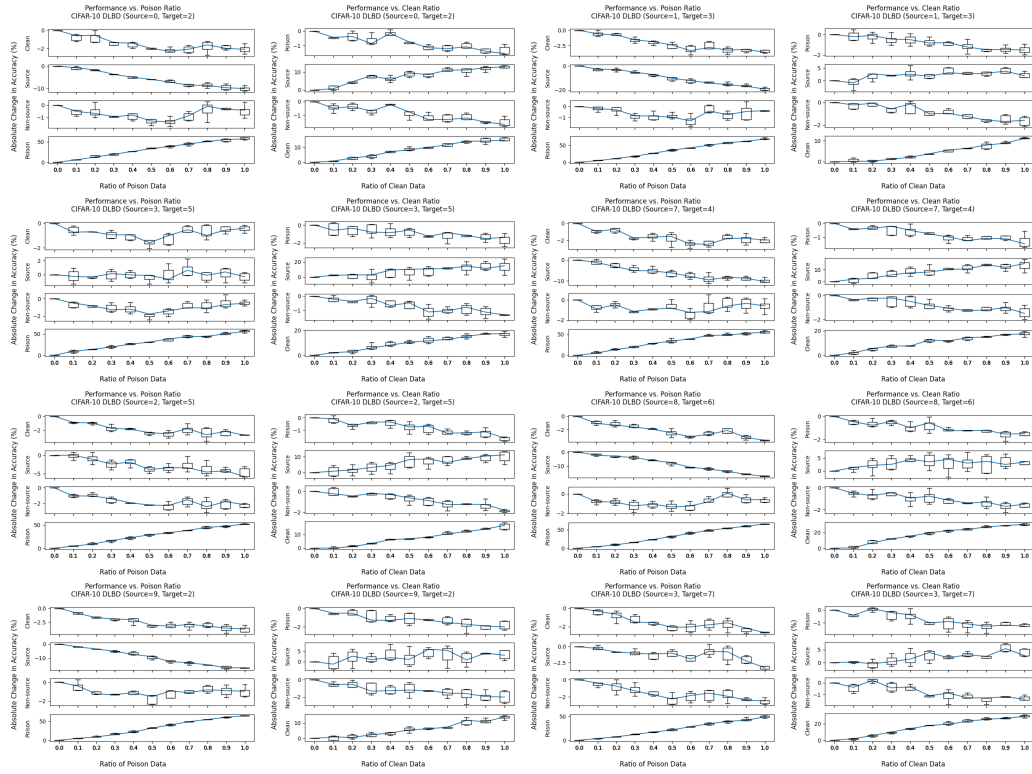


Figure 14: Full compatibility results for the WATERMARK attack on CIFAR-10.

## D.2 DEFENSE EVALUATION

This section includes additional experimental results concerning the performance of our defense. Tables 2-8 display the unabridged results of our main evaluation results for our defense. In particular, Table 2 also includes results of the three baseline defenses for the standard 1-to-1 DLBD attack on CIFAR-10.

We note that even though we have selected 1% as the threshold for a “successful” defense, in many of the failure cases, **ISPL+B** still achieves relatively low TMR. For instance, setting the threshold to 5% increases the number of successful scenarios to 142 (compared to 134 at 1%, out of 165 total).

Additionally, we observe in Table 2 that our clean accuracy is comparable to (or even slightly better than) that of Activation Clustering (**AC**), the next best defense, despite achieving significantly lower TMR in our evaluations.

Table 2: Performance on the CIFAR-10 DLBD scenario (1-to-1) using the PreActResNet18 architecture. The S / T column lists the CIFAR-10 source and target classes.  $\epsilon$  refers to the percentage of the source class which is poisoned. For the remainder of the columns, the top level column headers give the defense type: **Oracle** (training only on clean data), **ND** (no defense), **SS** (spectral signatures), **AC** (activation clustering), **ITLM** (iterative trimmed loss minimization, and **ISPL+B** (ISPL + boosting, this work); the second level column headers give the metric type: C (clean accuracy, higher is better), A (targeted misclassification rate, lower is better), FP (false positives, lower is better), FN (false negatives, lower is better). Successful runs (TMR < 1%) are highlighted.

S / T	$\epsilon$	<b>Oracle</b>		<b>ND</b>		<b>SS</b>		<b>AC</b>		<b>ITLM</b>		<b>ISPL+B</b>			
		C	A	C	A	C	A	C	A	C	A	C	A	FP	FN
0 / 2	5	93.3	0.0	93.1	17.2	92.5	2.1	90.3	0.1	92.5	4.7	90.9	0.0	3761	23
	10	93.1	0.0	92.8	42.6	91.3	18.2	90.7	14.7	92.5	43.7	90.6	0.0	3811	22
	20	93.1	0.0	92.4	79.8	89.5	4.6	90.3	23.9	92.1	59.4	90.7	0.2	3773	118
1 / 3	5	93.1	0.0	92.7	1.4	92.4	0.3	90.6	0.3	92.6	0.0	90.9	0.0	3787	2
	10	93.0	0.0	92.4	11.1	91.3	1.1	90.3	0.4	92.3	7.7	90.8	0.0	3758	5
	20	93.1	0.0	92.5	55.7	88.2	4.3	90.0	4.8	92.2	51.6	90.6	0.0	3819	5
2 / 5	5	93.1	0.8	92.9	81.7	92.8	81.7	89.4	73.5	92.8	81.0	90.5	1.2	3778	44
	10	93.3	0.9	92.9	83.3	92.1	81.0	90.4	76.2	92.5	82.1	90.6	0.6	3928	47
	20	93.0	0.8	92.9	81.2	88.2	72.9	90.9	76.2	92.4	77.9	90.8	74.4	3552	981
3 / 5	5	93.2	0.2	92.8	72.9	92.6	69.9	91.0	56.5	92.8	68.0	90.8	0.6	3843	26
	10	93.1	0.2	92.9	86.6	91.8	76.8	90.8	76.7	92.8	87.6	91.0	0.4	3759	42
	20	93.1	0.2	92.8	89.3	90.2	81.7	90.4	80.6	92.7	88.9	90.4	0.2	3925	59
3 / 7	5	93.1	0.2	92.9	8.0	92.3	2.0	90.0	0.8	92.8	0.3	90.9	0.1	3656	12
	10	92.9	0.0	92.8	46.6	91.3	20.8	89.7	3.4	92.4	36.5	90.7	0.1	3725	19
	20	93.0	0.0	92.5	60.8	88.6	36.0	90.7	59.1	92.4	73.3	90.3	0.2	3895	100
7 / 4	5	93.0	0.0	93.2	76.2	92.5	58.2	90.7	15.6	92.6	40.6	91.0	0.0	3729	2
	10	93.1	0.0	93.3	87.8	92.0	80.1	90.3	72.5	92.6	84.2	90.7	0.0	3781	3
	20	93.2	0.0	93.1	92.9	88.8	36.3	90.6	74.0	92.6	91.1	90.8	0.0	3637	8
8 / 6	5	93.1	0.0	93.0	3.0	92.5	1.3	89.6	0.3	92.9	0.6	90.8	0.0	3818	2
	10	93.3	0.0	93.1	87.8	91.2	47.0	91.0	2.9	92.3	15.3	90.6	0.0	4018	2
	20	93.2	0.0	93.1	93.2	89.3	7.4	90.4	62.1	92.5	89.4	91.0	0.0	3697	4
9 / 2	5	93.3	0.0	92.9	75.4	92.7	14.5	90.3	31.0	92.7	1.0	91.0	0.0	3625	4
	10	93.1	0.0	93.0	83.0	91.8	77.6	90.9	79.8	92.6	81.2	90.8	0.2	3718	37
	20	93.0	0.0	92.3	41.2	89.4	76.6	91.1	78.5	92.6	81.2	90.6	0.2	3699	74

Table 3: Performance on the CIFAR-10 DLBD scenario (all-to-1) using the PreActResNet18 architecture. The T column lists the target class (i.e., all poisoned images have label T). Each of the 9 source classes contain  $\epsilon/9$  percent poison.

T	$\epsilon$	Oracle		ND		ISPL+B			
		C	A	C	A	C	A	FP	FN
2	5	93.2	0.0	93.0	0.1	91.1	0.0	3624	9
	10	93.1	0.1	93.0	0.8	90.9	0.0	3632	25
	20	93.3	0.0	92.3	74.2	90.6	0.1	3770	49
3	5	93.1	0.1	92.7	0.2	90.6	0.1	3921	8
	10	93.0	0.1	92.4	25.4	90.6	0.1	3855	24
	20	93.3	0.1	92.8	87.6	90.3	0.1	3947	67
5	5	93.2	0.2	93.0	62.8	90.8	0.1	3682	6
	10	93.0	0.2	93.1	92.2	90.7	0.1	3764	21
	20	93.2	0.1	92.9	92.1	90.9	0.5	3698	66
7	5	93.3	0.1	93.0	76.2	90.9	0.2	3605	8
	10	93.0	0.1	92.8	83.3	90.8	0.2	3542	21
	20	93.0	0.1	92.8	89.1	90.9	0.5	3592	39

Table 4: Performance on the CIFAR-10 DLBD scenario (all-to-all) using the PreActResNet18 architecture. The  $S \rightarrow T$  column lists offset of the cyclic permutation (i.e., 2 means that source class 0 is poisoned as target class 2, source class 1 is poisoned as target class 3, etc.).  $\epsilon$  refers to the percentage of the source class which is poisoned.

$S \rightarrow T$	$\epsilon$	Oracle		ND		ISPL+B			
		C	A	C	A	C	A	FP	FN
2	5	92.7	0.0	92.4	78.0	90.3	0.1	3790	130
	10	92.8	0.0	92.5	87.8	90.0	0.1	3648	256
	20	92.2	0.1	92.6	88.2	88.2	0.2	3695	821
3	5	92.8	0.0	93.2	88.2	90.6	0.0	3664	58
	10	92.5	0.0	92.9	89.7	89.6	0.0	3892	172
	20	92.2	0.0	92.6	90.7	88.4	0.1	3902	384
5	5	93.1	0.0	93.0	90.1	90.7	0.1	3446	57
	10	92.8	0.0	93.2	90.6	90.4	8.9	3416	410
	20	92.4	0.1	92.9	91.0	90.3	88.5	3367	9027
7	5	93.1	0.1	93.1	85.6	90.6	0.1	3505	58
	10	92.7	0.0	93.2	89.0	90.6	69.4	3532	3576
	20	92.5	0.0	93.2	90.0	90.6	86.7	3076	8952

Table 5: Performance on the CIFAR-10 WATERMARK scenario (1-to-1) using the PreActResNet18 architecture. The S / T column lists the CIFAR-10 source and target classes.  $\epsilon$  refers to the percentage of the source class which is poisoned.

S / T	$\epsilon$	Oracle		ND		ISPL+B			
		C	A	C	A	C	A	FP	FN
0 / 2	5	93.1	0.2	93.3	75.2	90.8	0.4	3826	13
	10	93.2	0.3	93.2	84.5	90.6	4.4	3868	54
	20	93.1	0.1	93.0	87.0	90.6	76.8	3741	787
1 / 3	5	93.1	0.0	93.0	47.7	90.8	0.0	3752	2
	10	93.0	0.0	93.1	74.4	90.8	0.0	3746	5
	20	93.2	0.0	92.9	85.8	90.9	0.0	3634	11
2 / 5	5	93.0	2.0	93.0	45.2	90.7	11.9	3685	109
	10	93.1	2.4	92.9	64.4	90.7	7.1	3664	122
	20	93.1	2.4	92.9	73.7	90.4	35.4	3499	622
3 / 5	5	93.0	0.1	93.0	45.1	90.6	0.2	3814	35
	10	93.1	0.1	93.0	74.3	90.8	0.3	3715	44
	20	92.9	0.5	92.9	85.1	90.4	21.7	3796	289
3 / 7	5	93.2	0.7	92.9	84.2	90.7	6.5	3920	16
	10	93.1	0.9	92.9	85.9	90.7	73.5	3717	406
	20	93.3	1.2	92.9	86.1	91.0	74.9	3772	928
7 / 4	5	92.9	0.0	93.1	77.6	90.8	0.0	3877	4
	10	92.9	0.0	92.9	82.9	90.7	0.0	3756	5
	20	93.0	0.0	92.9	89.4	90.6	72.4	3907	711
8 / 6	5	93.1	0.0	93.1	82.4	90.7	0.0	3639	1
	10	93.2	0.0	93.2	87.7	90.7	0.1	3751	3
	20	93.1	0.0	93.2	92.5	90.5	83.2	3795	859
9 / 2	5	93.1	0.3	93.1	69.6	91.0	0.8	3634	18
	10	92.9	0.1	92.9	75.0	90.7	0.4	3707	17
	20	92.9	0.2	92.8	78.8	90.6	1.3	3519	58



Table 6: Performance on the CIFAR-10 CLBD scenario using the PreActResNet18 architecture. The T column lists the target class (i.e., all poisoned images have label T).  $\epsilon$  refers to the percentage of the target class which is poisoned.

M	T	$\epsilon$	Oracle		ND		ISPL+B			
			C	A	C	A	C	A	FP	FN
GAN	0	5	93.2	0.0	93.2	0.1	90.9	0.1	3654	192
		10	93.1	0.0	93.0	0.1	90.9	0.1	3763	406
		20	93.1	0.0	93.3	0.3	91.0	0.2	3688	968
	2	5	93.0	0.1	93.2	1.3	90.7	0.2	3635	129
		10	92.9	0.1	92.9	12.1	90.7	0.4	3739	324
		20	93.1	0.1	93.3	27.2	90.8	4.3	3621	907
	4	5	92.9	0.1	93.3	0.2	90.9	0.1	3666	204
		10	92.9	0.1	93.0	0.4	90.8	0.1	3735	406
		20	92.9	0.0	93.1	3.4	91.0	0.3	3532	875
	7	5	93.1	0.0	93.2	0.5	90.9	0.0	3763	124
		10	93.3	0.0	93.3	4.8	90.6	0.1	3832	217
		20	92.9	0.0	93.0	25.2	90.8	0.2	3595	574
	9	5	93.2	0.0	93.0	0.3	91.0	0.1	3742	143
		10	93.1	0.1	93.1	4.7	90.9	0.1	3663	400
		20	93.1	0.0	93.2	10.6	90.7	0.7	3943	913
$\ell_2$	0	5	93.0	0.0	93.2	0.3	90.8	0.0	3633	162
		10	93.2	0.0	93.1	6.1	90.6	0.1	3747	351
		20	92.9	0.0	93.2	45.8	90.6	1.1	3848	757
	2	5	92.9	0.0	93.2	30.1	91.0	0.2	3694	95
		10	93.2	0.1	93.1	68.9	90.4	0.2	3877	219
		20	92.9	0.1	93.1	76.4	90.6	20.3	3716	633
	4	5	93.0	0.1	93.5	6.8	90.9	0.1	3639	140
		10	93.0	0.1	93.0	57.4	90.6	0.5	3793	299
		20	93.0	0.0	93.1	74.4	90.2	4.8	3731	587
	7	5	92.9	0.0	93.0	0.3	91.0	0.1	3769	157
		10	93.3	0.0	92.9	22.1	90.7	0.1	3796	366
		20	92.9	0.0	93.1	68.0	90.5	0.4	3932	732
	9	5	93.1	0.1	93.1	0.4	91.0	0.1	3871	174
		10	93.4	0.1	93.2	12.5	90.6	0.1	3846	332
		20	92.9	0.0	93.1	68.6	90.9	0.9	3622	731
$\ell_\infty$	0	5	93.2	0.0	93.1	0.5	91.1	0.0	3732	109
		10	93.1	0.0	93.0	3.8	91.1	0.1	3591	301
		20	93.2	0.0	93.1	51.3	90.7	0.2	3686	729
	2	5	93.1	0.1	93.2	13.7	90.8	0.1	3723	44
		10	93.3	0.1	93.3	52.9	90.9	0.2	3641	120
		20	93.0	0.1	93.0	66.2	90.4	1.0	4157	430
	4	5	93.1	0.1	93.2	0.6	90.7	0.1	3919	67
		10	93.2	0.1	93.1	14.4	90.8	0.1	3918	183
		20	93.1	0.0	93.1	4.1	90.6	0.2	3807	716
	7	5	93.2	0.0	93.0	1.0	90.6	0.0	3592	97
		10	93.2	0.0	93.0	32.6	90.6	0.1	3780	235
		20	93.0	0.0	93.1	67.4	90.5	0.2	3625	492
	9	5	93.1	0.1	93.1	0.7	91.0	0.1	3683	109
		10	93.1	0.0	93.1	3.7	90.6	0.2	3929	308
		20	93.2	0.1	93.4	1.0	90.7	0.2	3697	792

Table 7: Performance on the GTSRB DLBD scenario (1-to-1) using the ResNet32 architecture. The S / T column lists the GTSRB source and target classes.  $\epsilon$  refers to the percentage of the source class which is poisoned.

S / T	$\epsilon$	Oracle		ND		ISPL+B			
		C	A	C	A	C	A	FP	FN
0 / 2	5	94.2	0.0	94.4	0.0	95.1	0.0	628	0
	10	94.9	0.0	94.2	0.0	94.8	0.0	591	0
	20	94.4	0.0	94.4	0.0	94.1	0.0	558	1
1 / 2	5	93.9	0.0	94.5	0.1	94.4	0.0	327	1
	10	94.3	0.0	94.5	0.1	94.3	0.0	430	8
	20	94.2	0.0	93.7	53.2	93.7	0.1	418	25
1 / 0	5	94.5	0.0	94.1	87.5	94.3	0.0	582	0
	10	94.0	0.0	94.6	97.6	94.5	0.0	460	6
	20	94.2	0.0	94.5	97.9	93.0	82.6	569	79
2 / 13	5	94.2	0.0	94.5	91.9	94.2	89.7	269	75
	10	94.3	0.0	94.8	97.5	94.7	95.7	366	150
	20	94.2	0.0	93.8	96.8	93.9	98.1	472	300
38 / 4	5	94.5	0.0	94.1	1.6	94.2	4.9	453	69
	10	94.1	0.0	92.7	3.0	93.8	2.3	668	138
	20	94.6	0.0	94.1	9.3	93.7	30.1	665	276
31 / 24	5	94.3	0.0	94.0	47.4	95.2	0.0	616	0
	10	94.2	0.0	93.5	60.7	93.8	0.0	553	0
	20	93.9	0.0	93.9	83.0	94.7	0.0	643	7
15 / 29	5	94.5	0.0	94.5	0.5	94.1	0.0	674	7
	10	94.3	0.0	94.4	0.5	94.5	0.0	649	10
	20	94.1	0.0	94.4	0.0	94.6	0.5	706	74
9 / 18	5	92.8	0.0	93.8	61.9	94.3	0.0	586	2
	10	93.8	0.0	94.6	96.9	94.4	0.0	607	2
	20	94.3	0.0	94.2	98.8	94.3	0.0	586	26

Table 8: Performance on the GTSRB WATERMARK scenario (1-to-1) using the ResNet32 architecture. The S / T column lists the GTSRB source and target classes.  $\epsilon$  refers to the percentage of the source class which is poisoned.

S / T	$\epsilon$	Oracle		ND		ISPL+B			
		C	A	C	A	C	A	FP	FN
0 / 2	5	94.6	0.0	94.5	0.0	93.0	0.0	369	0
	10	94.4	0.0	93.8	0.0	94.0	0.0	416	0
	20	94.1	0.0	94.1	0.0	93.7	0.0	783	4
1 / 2	5	94.4	0.0	94.5	10.3	94.2	0.0	452	1
	10	94.1	0.0	94.2	54.0	94.7	0.0	359	8
	20	94.5	0.0	94.1	77.5	94.2	0.0	747	17
1 / 0	5	94.2	0.0	94.1	0.6	93.7	0.0	379	0
	10	94.9	0.0	94.2	10.7	94.3	0.0	305	5
	20	94.9	0.0	94.5	73.3	93.1	0.6	360	80
2 / 13	5	94.5	0.0	94.1	1.6	94.7	0.0	270	0
	10	93.7	0.0	93.9	32.1	94.8	0.0	278	0
	20	94.4	0.0	94.0	76.9	94.2	0.1	401	300
38 / 4	5	94.4	0.0	94.2	50.0	93.9	0.0	308	0
	10	94.2	0.0	93.3	65.4	94.3	0.0	273	0
	20	94.2	0.0	94.2	78.1	94.0	66.4	685	275
31 / 24	5	94.4	0.0	94.5	69.3	94.0	0.0	378	0
	10	94.6	0.0	94.7	81.1	94.3	0.0	292	0
	20	94.8	0.0	94.5	80.4	94.4	0.0	566	8
15 / 29	5	94.4	0.0	94.5	1.0	94.2	0.0	302	0
	10	94.5	0.0	94.1	0.5	94.6	0.0	344	0
	20	94.4	0.0	94.5	47.6	94.4	19.0	482	59
9 / 18	5	93.9	0.0	93.8	6.9	94.3	0.0	331	0
	10	94.3	0.0	94.3	75.0	94.3	0.0	269	0
	20	94.8	0.0	94.6	94.0	94.2	0.0	482	0

Table 9: Performance on the CIFAR-10 DLBD scenario using the PreActResNet18 architecture with an adaptive attack. The S / T column lists the CIFAR-10 source and target classes.  $\epsilon$  refers to the percentage of the source class which is poisoned.

S / T	$\epsilon$	ISPL+B			
		C	A	FP	FN
0 / 2	5	90.6	0.0	3899	23
	10	91.0	0.0	3594	17
	20	90.6	0.2	3819	78
1 / 3	5	90.9	0.0	3733	1
	10	91.0	0.0	3796	4
	20	90.8	0.0	3797	17
2 / 5	5	90.7	0.9	3741	46
	10	90.8	64.5	3656	336
	20	90.6	74.0	3558	953
3 / 5	5	90.8	0.3	3562	10
	10	90.7	8.2	3665	51
	20	90.4	69.4	4162	731
3 / 7	5	90.6	0.1	3665	6
	10	90.6	0.1	3754	23
	20	90.6	0.3	3526	46
7 / 4	5	90.8	0.0	3746	1
	10	91.0	0.0	3730	2
	20	90.8	0.0	3559	11
8 / 6	5	90.7	0.0	3760	2
	10	90.9	0.0	3723	5
	20	90.7	0.0	3818	4
9 / 2	5	90.8	0.0	3738	11
	10	90.9	0.1	3660	21
	20	90.8	0.4	3640	70

#### D.2.1 ADAPTIVE ATTACKER

The attacks used in the main experiments are oblivious to the presence of a defender when selecting the data to poison. In this section, we devise an strong adaptive attacker with white-box access to the ISPL algorithm when constructing the poisoned dataset.

The success of the defense rests crucial on the partition of training data returned by the ISPL algorithm. In order for the boosting phase to succeed, the partition should consist of homogeneous sets, i.e., the poison must be concentrated in a small number of sets within the partition; hence, the adaptive attacker’s objective is to try and distribute the poisoned samples across multiple sets.

In particular, rather than randomly selecting a  $\epsilon$  fraction of the source class to poison, an adaptive attacker with white-box access to the defense can first run the ISPL algorithm (using the same parameters) on the clean dataset to create a partition of the dataset, then random select a  $\epsilon$  fraction *from each partition* to poison. The idea is that if the ISPL algorithm returns a similar partition, then the poison will be still be distributed across multiple sets, thereby breaking the defense.

Table 9 presents the results of our defense against the strong adaptive attacker described above. Against the adaptive attack, our defense still succeeds in 20/24 of the scenarios (versus 22/24 for the standard oblivious attack). These results suggest the ISPL algorithm remains robust even to white-box adaptive attacks.

## D.2.2 VARYING THE TRAINING SETUP

As prior works (Schwarzschild et al., 2021) have observed that results in data poisoning, particularly with DNNs, can vary significantly with the training setup, we additionally ran our defense (along with the three baseline defenses) on the standard CIFAR-10 DLBD attack using both the PreActResNet18 and ResNet32 models, respectively, and report results after training for 200 epochs (instead of 100, as in our main experiments).

Tables 10 and 11 report the results of these experiments. We observe that the defense success rates are largely consistent with those in the main experiments across all defenses; the biggest change is that the Spectral Signatures defense successfully defends against 9 scenarios instead of just 1 (out of 24 total). **ISPL+B** still achieves the best performance in terms of reducing the targeted misclassification rate below 1% (with a 2-3% drop in clean accuracy).

Table 10: Performance on the CIFAR-10 DLBD scenario (1-to-1) using the PreActResNet18 architecture, when training for the final model for 200 epochs. The S / T column lists the CIFAR-10 source and target classes.  $\epsilon$  refers to the percentage of the source class which is poisoned.

S / T	$\epsilon$	Oracle	ND		SS				AC				ITLM				ISPL+B			
		A	C	A	C	A	FP	FN	C	A	FP	FN	C	A	FP	FN	C	A	FP	FN
0 / 2	5	1.3	94.5	91.3	94.5	79.9	7381	130	91.9	58.3	18926	155	94.6	84.9	994	244	92.8	0.0	3640	23
	10	1.3	94.1	90.6	94.5	66.0	7383	383	92.3	85.9	19790	320	94.2	92.8	1961	461	92.8	0.0	3479	25
	20	1.1	94.6	80.2	94.2	64.2	14335	335	92.4	73.9	19127	601	93.8	93.8	3897	897	91.6	22.9	3711	237
1 / 3	5	0.0	94.4	92.9	94.7	5.5	7319	68	90.9	19.5	19791	155	94.8	96.5	986	236	92.8	0.0	3434	2
	10	0.0	94.6	98.4	94.5	0.0	7035	35	92.5	68.7	19033	333	94.6	98.0	1981	481	93.0	0.0	3348	3
	20	0.0	94.4	99.6	94.6	0.0	14007	7	92.2	91.8	18317	622	94.4	99.4	3914	914	93.0	0.0	3253	2
2 / 5	5	1.1	94.4	80.4	94.6	76.4	7494	243	92.4	53.9	19937	172	94.7	79.4	985	235	92.6	0.2	3704	5
	10	0.9	94.4	97.2	94.4	0.1	7053	53	92.9	81.8	18657	313	94.7	92.4	990	490	92.9	0.2	3200	16
	20	1.2	94.4	94.0	94.5	87.7	14263	263	92.6	89.4	20531	406	94.6	95.4	966	966	92.8	0.3	3540	38
3 / 5	5	7.6	94.7	91.0	94.7	88.5	7281	30	92.6	90.8	19172	172	94.5	91.4	993	243	92.8	81.1	3693	167
	10	5.9	94.8	94.0	94.4	8.6	7014	14	92.3	91.6	20293	296	94.6	92.3	988	488	92.6	90.2	3355	496
	20	7.6	94.7	90.8	94.3	90.6	14092	92	92.6	92.6	18236	652	94.7	91.7	974	974	92.6	87.4	3210	995
3 / 7	5	0.6	94.3	33.8	94.6	98.3	7500	249	91.9	97.2	21289	246	94.7	98.4	995	245	92.7	0.0	3692	5
	10	0.7	94.4	98.5	94.6	96.6	7135	135	92.2	98.2	20630	484	94.5	98.6	1979	479	92.7	2.4	3427	22
	20	0.7	94.4	98.5	93.7	78.5	14675	675	92.3	98.2	20470	987	94.4	98.9	980	980	92.9	10.5	3259	43
7 / 4	5	1.5	94.7	92.0	94.6	0.6	7280	29	92.3	39.2	19353	150	94.8	91.6	992	242	92.8	0.5	3258	30
	10	1.5	94.6	94.7	94.4	0.0	7023	23	92.0	47.9	19631	285	94.4	94.5	1979	479	93.0	0.3	3627	293
	20	1.5	94.6	96.5	94.3	0.1	14000	0	92.1	78.6	21292	22	94.4	96.5	3910	910	92.8	84.5	3203	867
8 / 6	5	0.2	94.7	97.0	94.8	80.5	7470	219	92.8	73.3	19293	152	94.5	98.3	993	243	92.8	0.0	3494	2
	10	0.2	94.4	99.5	94.7	0.0	7008	8	92.6	97.6	19544	288	94.4	99.4	1981	481	92.9	0.0	3571	1
	20	0.2	94.7	99.5	94.4	0.0	14000	0	92.5	96.4	18946	597	94.2	99.5	3908	908	92.6	0.2	3492	8
9 / 2	5	0.1	95.0	92.0	94.4	93.3	7501	250	91.7	85.0	23573	151	94.6	97.3	988	238	93.0	0.0	3291	2
	10	0.1	94.5	93.9	94.3	93.1	7500	500	92.1	95.1	22896	251	94.4	98.6	1970	471	93.1	0.0	3133	1
	20	0.1	94.4	96.1	94.7	0.0	14010	10	93.1	98.9	18651	575	94.1	99.0	3906	906	93.1	0.0	3223	2

Table 11: Performance on the CIFAR-10 DLBD scenario (1-to-1) using the ResNet32 architecture, when training for the final model for 200 epochs. The S / T column lists the CIFAR-10 source and target classes.  $\epsilon$  refers to the percentage of the source class which is poisoned.

S / T	$\epsilon$	Oracle	ND		SS				AC				ITLM				ISPL+B			
		A	C	A	C	A	FP	FN	C	A	FP	FN	C	A	FP	FN	C	A	FP	FN
0 / 2	5	1.1	92.6	85.0	91.8	57.3	7499	248	88.8	0.6	24211	133	91.8	83.3	988	238	89.8	0.0	5752	31
	10	1.1	92.4	92.6	91.7	91.5	7422	422	88.8	78.6	24031	250	91.7	92.3	1969	469	89.5	0.0	5445	33
	20	1.5	92.5	94.9	90.4	64.2	14590	590	88.6	62.7	23686	455	91.9	94.2	3890	890	88.0	0.0	6992	86
1 / 3	5	0.1	92.7	98.5	91.7	5.7	7479	227	88.8	2.4	23903	125	91.9	12.7	988	238	89.8	0.0	5776	1
	10	0.1	91.6	35.0	91.1	3.3	7436	436	88.3	24.9	23891	254	92.0	69.2	988	488	89.8	0.0	5736	3
	20	0.0	92.1	98.1	91.5	0.0	14004	4	89.1	0.4	21145	70	91.9	97.3	3900	900	89.4	0.0	5833	1
2 / 5	5	1.7	92.2	62.7	91.2	43.2	7493	242	88.0	1.4	24001	128	92.2	75.7	994	244	88.8	0.1	6358	6
	10	1.6	92.5	92.4	91.9	89.8	7476	476	89.3	81.5	23827	275	91.6	93.2	1975	475	89.2	0.0	5985	26
	20	1.6	91.7	95.8	89.9	3.5	14349	349	88.5	87.2	21086	711	91.9	95.1	3905	905	89.8	0.2	5684	40
3 / 5	5	6.3	91.3	88.9	91.7	87.9	7466	215	88.9	80.0	23817	131	92.2	90.8	996	246	89.2	27.5	5974	59
	10	6.2	91.8	90.8	91.6	86.4	7348	348	88.7	73.1	21299	136	92.2	89.5	990	490	89.1	82.1	5681	344
	20	6.3	92.3	90.8	90.5	71.9	14090	90	89.3	78.5	20694	156	90.9	88.8	3918	918	89.8	86.7	5093	994
3 / 7	5	1.1	92.6	98.4	91.0	97.1	7452	201	86.2	72.8	23823	189	92.1	97.1	994	244	89.4	0.2	5498	13
	10	1.1	92.4	98.6	91.8	96.7	7315	315	88.6	96.2	23648	482	92.3	98.0	1981	481	89.8	0.0	5126	16
	20	1.1	92.9	98.6	90.9	97.0	14167	167	89.1	95.4	20600	551	92.4	98.1	3924	924	88.6	0.2	6642	26
7 / 4	5	1.7	92.1	88.5	91.6	87.5	7486	235	89.3	72.2	23928	149	92.4	92.2	992	242	88.8	0.4	6643	27
	10	1.7	92.7	93.9	91.9	94.2	7371	371	88.3	59.2	23753	193	92.1	96.2	1973	473	88.9	0.8	6478	32
	20	1.7	92.6	96.9	91.1	94.1	14397	397	88.2	47.6	23737	423	91.7	95.8	3904	904	88.6	46.9	6322	209
8 / 6	5	0.2	92.7	98.0	91.3	97.8	7441	190	89.1	88.7	23658	164	92.5	96.9	988	238	89.6	0.0	5991	0
	10	0.2	92.1	97.7	91.8	97.2	7089	89	90.2	95.1	19585	280	92.3	98.7	973	473	89.3	0.0	6007	2
	20	0.2	92.8	98.8	91.3	96.0	14297	297	87.2	64.2	23347	646	92.3	98.6	975	975	89.4	0.0	5691	3
9 / 2	5	0.1	92.9	93.2	91.2	93.2	7478	225	88.7	1.2	23518	136	92.1	94.0	991	241	90.3	0.0	5444	2
	10	0.1	92.6	98.6	91.4	94.7	7497	497	88.5	91.5	24034	242	92.5	97.8	986	486	88.1	0.0	7220	2
	20	0.1	92.6	97.4	90.5	0.0	14011	11	90.6	97.7	18658	578	91.9	99.2	3881	811	89.6	0.0	5742	1

### D.2.3 SENSITIVITY OF ISPL TO HYPERPARAMETERS

We next conduct some ablation studies to better understand the effects of the two main hyperparameters in Algorithm 2: the expansion factor  $\alpha$  and the subset size  $\beta$ . Computationally, larger  $\beta$  means fewer components and fewer outer iterations of ISPL (and is thus more efficient); in our main experiments, we use  $\beta = 1/8$  and run ISPL 8 times in sequence to generate 8 components. Additionally, when estimating the self-expansion error, a larger  $\alpha$  leads to lower variance estimates of the expansion error, but less effective measures of generalization; hence, we should prefer taking  $\alpha$  as large as possible to produce better estimates (until memorization effects take over). Our experiments use both  $\alpha = 1/2$  (for GTSRB, due to the imbalanced class sizes) and  $\alpha = 1/4$  (for CIFAR-10).

Tables 12 and 13 present our results from the ablation studies, conducted on a subset of the CIFAR-10 DLBD and CLBD subsets. We do not include the self-training step after ISPL as in the main experiments, in order to better highlight the trends. In particular, without self-training, we expect both lower clean accuracies and higher targeted misclassification rates due to not recovering all the compatible clean data.

Our main finding is that our method is quite robust to both the expansion factor  $\alpha$  and subset size  $\beta$ . In particular,  $\beta \in [1/8, 1/16]$  and  $\alpha \in [1, 1/4]$  all yield strong defenses with less than 10% targeted misclassification. As expected, increasing  $\beta$  leads to a stronger defense but lower clean accuracies. In particular,  $\beta = 1$  (which identifies only a single subset consisting of 96% of the original dataset) fails in all settings of  $\alpha$ ; this is the setting for which **ISPL+B** is conceptually the most similar to the **ITLM** defense, which offers a possibly explanation for **ITLM**'s poor performance in our experiments. Additionally,  $\alpha = 1$  avoids memorization, mainly because we do not train until convergence within the ISPL loop. Finally, we note that  $\alpha = 1/2$  appears to achieve a modest optimum, which is particularly noticeable when paired with smaller  $\beta$ .

Table 12: Average clean accuracies after running ISPL on three scenarios of CIFAR-10 DLBD and CLBD using the PreActResNet18 architecture, with various settings of  $\alpha$  and  $\beta$ .

$\alpha$	$\beta$					average
	1	1/2	1/4	1/8	1/16	
1	92.55	91.65	90.37	87.92	85.41	89.58
1/2	92.63	91.85	90.25	87.28	83.54	89.11
1/4	92.64	91.93	89.92	86.52	83.01	88.80
1/8	92.70	91.69	89.21	86.56	83.83	88.80
1/16	92.58	91.63	89.63	86.98	85.15	89.20
average	92.62	91.75	89.88	87.05	84.19	

Table 13: Average targeted misclassification rates after running ISPL on three scenarios of CIFAR-10 DLBD and CLBD using the PreActResNet18 architecture, with various settings of  $\alpha$  and  $\beta$ .

$\alpha$	$\beta$					average
	1	1/2	1/4	1/8	1/16	
1	29.21	15.38	12.06	5.88	7.43	13.99
1/2	30.52	15.74	12.26	3.54	4.18	13.25
1/4	39.15	15.12	11.10	7.07	9.59	16.41
1/8	36.54	21.99	12.71	10.96	10.78	18.60
1/16	37.15	26.31	12.60	11.91	11.67	19.93
average	34.51	18.91	12.15	7.87	8.73	